NTNU
Norwegian University of
Science and Technology

Preparation and Optimization of a Membrane for 3rd Generation Solvent Membrane Contactor

Asad Arif

Chemical Engineering
Submission date: July 2016
Supervisor: Liyuan Deng, IKP
Co-supervisor: Luca Ansaloni, IKP

Norwegian University of Science and Technology
Department of Chemical Engineering

Dedicated to Nature, it's Creator and My Parents

Acknowledgement

Abstract

Third generation solvent is a new class of CO_2 absorbents with a great potential in terms of reduction of the regeneration energy requirement for post combustion carbon capture, but their use at the industrial scale is limited by their high volatility. Membrane contactor technology is proposed as possible solution, but the membrane layer must be purposely designed in order to act as amine barrier, without negatively affecting the overall CO_2 mass transfer resistance. Teflon AF2400 has been reported to be a suitable membrane material, but an improvement of its properties is required to achieve better performance of the membrane contactor.

Herein, a systematic study was performed to investigate mass transport properties of the main components present in the separation process (CO_2, H_2O and amine molecules) in mixed matrix membranes (MMMs) based on Teflon AF2400. Different MMMs were prepared by inclusion of inorganic materials (graphene, reduced graphene oxide and ZIF-8) in the polymeric matrix. In particular, the effect of different loadings (from 2 to 10%) has been investigated. The obtained membrane were characterized in terms of morphology, through high-resolution scanning electron microscopy, and transport performances, through pure gas (CO_2 and N_2) permeation experiments. The membrane with higher nanoparticles loadings displayed promising results.

According to the CO_2 permeability results, the membrane obtained by embedding 7.5 wt % ZIF-8 within the matrix was selected for further characterization in terms of amine transmembrane flux. To this purpose a pervaporation setup was used, which allows the investigation of pure chemicals as well as liquid mixtures. The results obtained from pervaporation experiments showed that the MMM developed in this work was able to achieve a, an CO_2/amine ideal selectivity of 763 at 40 °C, 378 at 50 °C and 212 at 60 °C. In comparison with the pure polymer membrane, the CO2/amine selectivity of this MMM is almost 2 times higher at 40°C, and even further improvement is obtained at 60 °C.

In order to improve the understating of the fundamental transport mechanism of amines through polymer layer sorption experiments were performed at 35 °C for the pure components of the liquid mixtures (H_2O, DEEA and MAPA). The solubility for MAPA and DEEA was found to be always below 0.005 g/g_{pol} in an activity range that would correspond to the one in the liquid mixture. These low solubility values are in line with the low permeation rate for amines obtained from the pervaporation experiments.

Table of Contents

List of Tables

List of Figures

x

Abbreviations

3D3M	3 Molar DEEA & 3 Molar MAPA aqueous solution
30% MEA	5 Molar MEA aqueous solution
6FDA	4,4'-(Hexafluoroisopropylidene)diphthalic anhydride
AMP	2-Amino-2-methyl-1-propanol
CMS	Carbon Molecular Sieve
CNT	Carbon Nanotubes
CCS	CO_2 Capture and Storage
DEA	Diethanolamine
DEEA	Methyldiethanolamine
FFV	Fractional free volume
GO	Graphene oxide
LN_2	Liquid Nitrogen
MAPA	3-(methylamino) propylamine
MEA	Monoethanolamine
MDEA	Methyldiethanolamine
MMM	Mixed Matrix Membrane
MOF	Metal Organic Framework
PCC	Post Combustion Capture
PDMS	Polydimethylsiloxane
PEBAX	Poly(ether-block-amide)
PP	Polypropylene
PTFE	Polytetrafluoroethylene
PTMSP	Poly (trimethylvinylsilane)
PMP	Polymethylpentene
PVTMS	Poly (trimethylvinylsilane)

PPO	Poly (2, 6-dimethyl-1, 4-phenylene oxide)
RGO	Reduced graphene oxide
SEM	Scanning Electron Microscope
STP	Standard Temperature Pressure
VCR	Metal Gasket Face Seal
ZIF	Zeolitic Imidazolate Framework

Symbols

p_B	Break through pressure
γ	Surface tension
d_{max}	Maximum pore diameter
θ	Angle
σ	Surface tension
K_g	Gas mass transfer coefficient
K_m	Membrane mass transfer coefficient
K_l	Liquid mass transfer coefficient
E	Enhancement factor
K_G	Overall resistance in membrane contactor
δ_D	Dense layer thickness
$K_{m,nwp}$	Non-wetting porous membrane
ν_m	Molar volume
$K_{m,D}$	Dense membrane resistance
$K_{m,nwp}$	Non-wetting porous membrane resistance
ε	Porosity
J	Flux
P	Permeability
C	Amount absorbed
A	Membrane area
T	Temperature
R	Ideal Gas constant
l	Membrane thickness
V_d	Chamber volume
p	Pressure
α	Selectivity
P_A	Permeability of component A
P_B	Permeability of component A
ν_m	Molar volume
S	Solubility

g	Gravitational constant
ρ	Density
$\dfrac{dc_A}{dx}$	Concentration gradient
D_A	Diffusion coefficient of A
D_B	Diffusion coefficient of B
D_o	Pre-exponential constant
S_o	Pre-exponential constant
E_d	Activation energy of diffusion
ΔH_s	Heat of solution
E_p	Energy of permeation
Δp	Pressure difference
$\dfrac{dp}{dt}$	Transmembrane flux
w	weight of permeate sample
M_i	Initial mass
$M_{i,\infty}$	Final equilibrium mass
μm	micrometer
mol	Mole
cm^2	centimeter square

1 Introduction

Nowadays, the increasing energy demand is principally addressed through the exploitation of fossil fuels, such as oil, coal and natural gas. However, the combustion of fossil fuels is responsible for the release of greenhouse gases in the atmosphere to the largest extent and for the consequent climate changes. Among the others, CO_2 represents the biggest portion of greenhouse gases and in the past few decades the development of technologies able to limit CO_2 emissions from anthropogenic sources has become a major field of interest.

At present, there are three possible approaches that are being studied for carbon capture: pre or post combustion capture and oxy-fuel combustion [1]. Out of these three, post-combustion capture (PCC) is fundamental to meet the 2°C scenario and avoid severe climate changes because it can be retrofitted in already existing plants [2]. However, PCC still faces few challenges, such as low CO_2 concentration in flue gas (13%) and large gas volume that must be treated. These factors can increase the investment and operating costs and decrease efficiency [1].

Among PCC processes, the main emphasis relies on amine scrubbing, reflecting the fact that industry's knowledge and overall process experience are both heavily slated towards absorption (largely used for H_2S removal, for instance). In a conventional absorption process (Figure 1), there is an absorber unit, where the liquid phase (amine-based absorbent) is brought in contact with the flue gas stream that needs purification, and a desorber unit, where the CO_2 is stripped out of the liquid phase, allowing its regeneration. The first process for removal of carbon dioxide from flue gases through amine-based solvents was patented in 1930 [3].

Even though amine-based absorption remains the benchmark for post-combustion applications, the development of more cost-effective technology is required in order to make the process more economically feasible. In particular, the energy requirement for the amine regeneration is still a challenge, as it can increase the overall energy production cost to a significant extent.
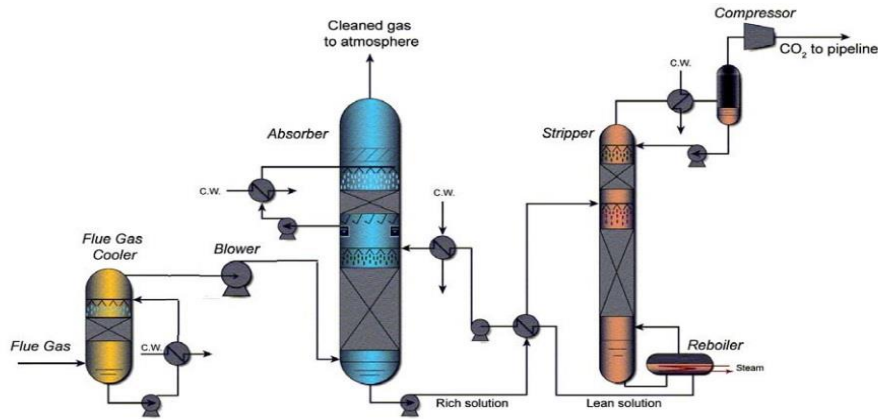
Figure 1: Typical amine absorption Process [4]

Recently, hybrid processes (membrane contactor) gained more attention in this field, as they are able to combine the advantages of different technologies [5], [6]. In membranes contactors, a polymeric layer (i.e., the membrane) acts as interface between the liquid and the gas phase. **Figure 2** shows the working scheme of a membrane contactor. This configuration offers several advantages compared to traditional absorption columns. For example, membrane contactors ensure a larger interface surface per unit volume (i.e., smaller footprint) and this area remains constant at different operating conditions, because the two fluid flows are independent. In comparison, absorption columns show flooding at large flow rates and unloading at lower rates. Furthermore, a linear relationship exists between capacity and modules, so capacity can easily be increased by adding more modules. This easier scalability allows membrane contactors to be operated in a wide range of capacities [7].
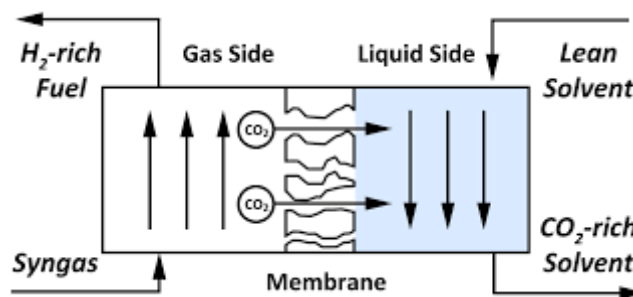
Figure 2: Depiction of membrane contactor [8]

In order to have a reduced effect on the overall CO_2 mass transfer coefficient, the membrane must be designed to be able to ensure high CO_2 transmembrane flux. Initially, porous materials

2

have been chosen as membrane layer at the gas-liquid interface, as they were able to ensure high transmembrane flux for the gas phase and thus reduced impact on the mass transfer coefficient. However, they can be affected by pore wetting, which can reduce the mass transfer coefficient [1]. The most common hydrophobic porous membranes are polypropylene (PP) and polytetrafluoroethylene (PTFE), typically produced as hollow fibers module [9]. The selection of the absorbent phase plays also an important role in pore wetting, as this phenomenon is influenced by the surface tension of the liquid and the contact angle between the liquid and the polymeric materials.

Recently, a new class of absorbents (i.e., 3rd generation solvents) have been developed which require lower regeneration energy and promise a lower energy penalty associated with the capture process. However, their use in traditional columns is limited due to their high volatility, which would tremendously increase the amine emissions in the atmosphere. Membrane contactors offer a suitable solution for the full exploitation of these new absorbents, especially if the membrane layer is purposely engineered in order to limit the transport of the organic compounds toward the gaseous phase.

1.1 Research Objective

During the master's specialization project, compatibility tests with 3rd generation solvents were carried out for different porous and dense membrane materials. Among porous membranes, polypropylene (PP) and polytetrafluoroethylene (PTFE) should the best compatibility, but long-term analysis (5 weeks) revealed high absorbent uptake and morphological changes in PTFE membrane. It was concluded wetting phenomena were likely to happen in these materials, so their use as membrane interface were not allowed. However, they could have been used as porous support for thin composite membrane preparation. Dense materials (Teflon AF 1600 & 2400 and PDMS) were also investigated. In this case, good chemical stability was achieved only by the Teflon AF polymer family [10].According to the larger CO_2 permeability; Teflon AF2400 was chosen as suitable membrane materials and characterized in terms of ability of act as amine barrier [11].

This master thesis is a part of the 3rd Generation Membrane Contactors (3GMC) project, supervised by Assoc. Prof. Liyuan Deng and Dr. Luca Ansaloni. The aim of the present task is to further characterize selected material and improve its properties by lowering the flux of 3rd generation solvents through the inclusion of nanoparticle in the membrane matrix. For this

reason, mixed matrix membranes prepared with different inorganic nanoparticles have been investigated in terms of mass transport properties, in order to identify the best candidates for the preparation of thin mixed matrix composite membranes that will be used as interface layer for the membrane contactor.

2 Background and Theory

2.1 Membrane Contactors

For post combustion capture of carbon dioxide, chemical absorption is considered the benchmark technology, and in particular, 30 wt% MEA aqueous solution is the reference for carbon dioxide absorption processes [12]. In literature, different amine-based systems have been investigated [13]. The main purpose of these studies was to select an amine based absorbent with a limited degradation over time, non-corrosive features, a high loading capacity, a high rate of reaction and a low energy requirement. Monoethanolamine (MEA), Diethanolamine (DEA), and Methyldiethanolamine (MDEA) are few notable amines that have been reported in literature [13].

The most recent research leads to development of the so-called 3rd generation amines e.g. 2-(diethylamino) ethanol (DEEA) and 3-(methylamino) propylamine (MAPA), which when utilized as mixture in solvent system show two phase behavior [14], as shown in Figure 3. The DEEA is a tertiary amine which contains ethyl groups on each side, can be manufactured from renewable sources and has showed good regeneration energy values. However, it shows low affinity for carbon dioxide and a slow kinetics. So, a secondary or primary amine is needed as an activator. On the other side, MAPA has high carbon dioxide absorption capacity and reaction rate. However, it also has a high-energy requirement for regeneration and it is difficult to strip. Combining the advantages of both amines, blends of DEEA and MAPA resulted in promising absorbents. These solvents form two immiscible phases upon carbon dioxide absorption, a CO_2 rich phase and a CO_2 lean phase [14]. The mixture is separated on the basis of density difference and rich phase goes to stripper for regeneration purpose and lean phase back to contactor. The stripper energy requirement would be lower based upon low solvent circulation. It has been claimed that this new class of absorbents can significantly reduce energy requirement in comparison with 5M MEA solution [13].

Figure 3: 5M MAPA/2M DEEA solution before and after CO_2 loading [15]

In membrane contactor, the membrane acts as an interface with the gas stream flowing on one side and the liquid stream on the other. Ideally, the membrane pores are gas-filled to ensure higher flux, but the solvent is kept at slightly higher pressure to avoid possible gas bubbling. However, recent studies showed that porous membranes are likely to suffer pore-wetting phenomena on long-term operations, which can significantly reduce the CO_2 mass transfer and have a negative effect on the overall performance of the contactor [9].

The Young-Laplace equation is a good tool to understand the pore wetting phenomenon in porous material, as it can provide a good approximation of the breakthrough pressure (p_B), the pressure required to force non-wetting fluid into the constricted regions of porous material [16], which can be applied to the liquid to enter the pores of the materials [17]:

$$p_B = -\frac{4\gamma cos\theta}{d_{max}}$$

where p_B is break through pressure, d_{max} is the pore diameter, γ is the surface tension and θ is the contact angle.

According to the indications given by the Young-Laplace equation, in order to have a positive value of the breakthrough pressure, the contact angle must be larger than 90°. In addition, larger value of p_B can be obtained either by decreasing the pore size of the membrane layer or using liquid with larger surface tension. Therefore, hydrophobic membranes with smaller pore size must be preferred for membrane contactors in which amine-based aqueous solution are used as liquid phase. Commonly, commercially available hydrophobic membranes are Polypropylene (PP) and Polytetrafluoroethylene (PTFE) [9]. Moreover, the selection of solvents also plays an important role in pore wetting, as the liquid with low surface tension can wet the surface.

6

Literature studies suggest that PTFE have higher contact angle and degradation is minimal with amine solvents on lab scale, although these studies are mainly focused on the use of MEA solution as liquid phase [9]. Typical values of surface tension and contact angle with porous membranes frequently used in membrane contactor applications are reported in the **Table 1**.

Table 1: Surface tension of aqueous amine solutions and their contact angle on porous membranes at 298 K
(Literature data from Ref [18], [19], [20], NTNU data from [10])

Solution	Amine Concentration (wt %)	Surface Tension σ (mN/m)	Contact Angle (°)	
			PP	PTFE
Water	--	72	117	135
Water (NTNU)	--	71	118.8	134.7
MEA	30	63.9	107	133
MEA (NTNU)	30	63.4	86.2	127.3
DEA	30	60.8	109.6	--
MDEA	30	53.5	121.6	--
AMP	30	46.1	113	130
3D3M (NTNU)	68	18.48	39.4	64.5

Chabanon et al. [12] suggested that even though PP membrane contactor shows promising results but it does not have chemical compatibility towards MEA in long term operations. Mavroudi et al. [21] observed 1.5-7% pore wetting in PP hollow membrane contactor with DEA and suggested that new membranes were needed that have higher hydrophobicity or new absorbents with higher surface tensions should be considered. On the other side, PTFE membranes are considered to be a better option due to their superior chemical stability and better resistance to pore wetting, in view of the high hydrophobicity. In another study, Chabanon et al. [22] investigated process intensification for post combustion carbon dioxide capture by increasing MEA concentration and temperature in PTFE membrane contactors. The study concluded that increasing MEA concentration up to 90% doesn't generate any operating problems, at least on short term operation. However, the main drawback is related to the high manufacturing cost.

As a result of intensive studies on membrane contactor for post combustion CO_2 capture applications, it was concluded that the porous membrane contactor should show the following characteristics: i) a high permeability to ensure high mass transfer compared to other carbon capture techniques; ii) the liquid does not have detrimental effect on membrane structure or wet the pores over the longer period of operation. From Table 1, it is also clear that in case 3rd

generation solvents (e.g., 3D3M) are used as liquid phase, porous materials can be easily wetted, in view of both the low surface tension of the liquid and the low contact angle with both PTFE and PP. Therefore, a new membrane design is needed which can ensure long and stable operation periods, without negatively affecting the CO_2 transmembrane flux.

A self-standing dense polymeric membrane was proposed. Polydimethylsiloxane (PDMS) [23] has been reported to have high permeability among amorphous polymers. Al-Saffar et al. [24] studied carbon dioxide removal from mix gas using dense (PDMS) and porous (PP) membrane contactor with 10% DEA aqueous solution. The permeability is inversely proportional to thickness, so the self-standing dense membrane of small thickness cannot provide high mass transfer coefficient in comparison with porous membrane.

In recent years, composite membranes were used as alternative to porous membrane in membrane contactors to deal with pore wetting and attain high mass transfer rates. A dense layer of highly permeable material is coated on porous material (support) to exploit benefits of both materials. The idea of composite membrane comes from gas separation membranes, where this has been investigated for more than three decades, but has only been recently applied to membrane contactors [25]. The characteristics of some notable polymeric materials used as dense layers in membrane contactor applications are reported in **Table 2**.

<div align="center">

Table 2 : Studies performed on dense polymeric membrane [25]

</div>

Polymer	CO_2 permeability	Membrane Type	System
PDMS	4500	Composite	CO_2/N_2
PVTMS	190	Asymmetric	CO_2/N_2
PMP	93	Composite	CO_2/N_2
PPO	50	Asymmetric	CO_2/CH_4
PTMSP	28,000	Composite	CO_2/N_2
Teflon AF 2400	3900	Composite	CO_2/N_2

From the theoretical point of view, the overall mass transfer coefficient in membrane contactor is expressed through the resistance-in-series model [17]. Three mass transfer coefficients are used for the description of the overall mass transfer resistance: the term related to the gas transport from the bulk phase to the membrane surface, the transport through membrane layer and transport through solvent boundary layer. Thus, the resistance-in-series model is described with the following equation [17]:

8

$$\frac{1}{K_G} = \frac{1}{K_g} + \frac{1}{K_m} + \frac{1}{mEk_l}$$

where K_g, K_m and K_l are mass transfer coefficient for gas, membrane and liquid respectively, E is enhancement factor (chemical reaction) and m is the solubility of the gas into the liquid at equilibrium. Membrane mass transfer coefficient K_m is different for gas filled pores and wet pores.
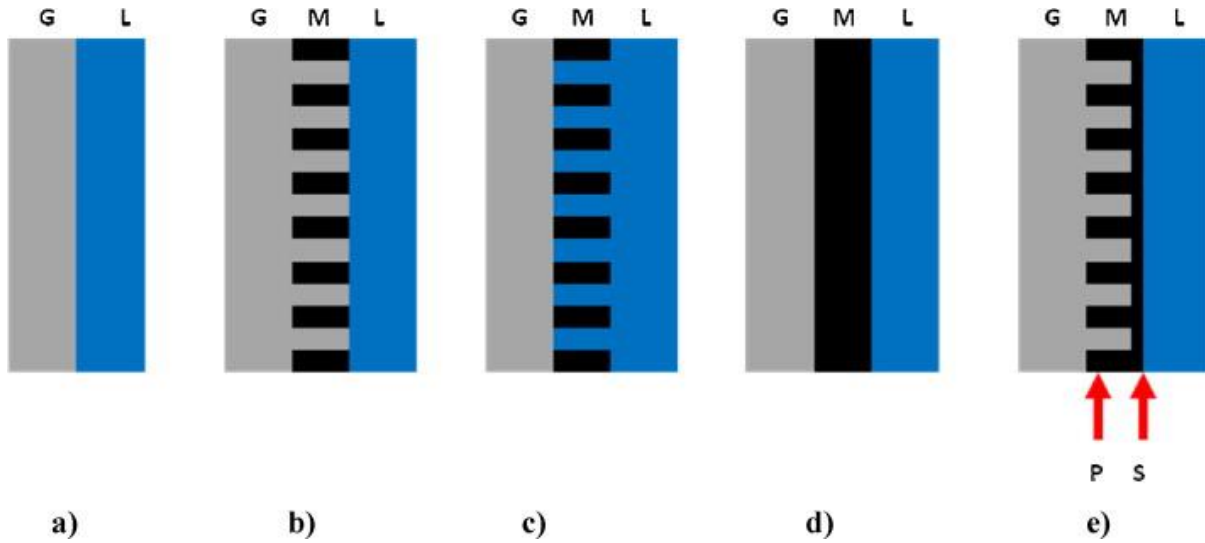
Figure 4: Schematic diagram mass transfer resistances of gas-liquid separations (reprinted from ref [25])

Figure 4 illustrates the resistance to mass transfer under different conditions. The term P is for porous membrane and S is for dense layer. The terms L, M, and G refers to liquid, membrane and gas phase. The image a) represents the packed column (direct contact between gas and liquid phase), b) porous membrane contactor (non-wetted), c) wetted porous membrane contactor, d) dense membrane contactor, e) composite membrane contactor with porous support and dense coating.

The composite membranes were used in hollow fibre modules to deal with pore wetting but coatings of dense layer on hollow fibre contribute to mass transfer resistance. The dense layer also allows selective transfer of species. For resistance in composite membrane contactor would be sum of resistance offered dense layer and porous layer [17].

$$\frac{1}{k_m} = \frac{1}{k_{m,nwp}} + \frac{1}{k_{m,D}}$$

9

$$\frac{1}{k_m} = \frac{\delta}{D_G \varepsilon} + \frac{\delta_D v_m}{PRT}$$

Where $K_{m,D}$ is dense membrane resistance, $K_{m,nwp}$ non-wetting porous membrane resistance, v_m is molar volume, δ is porous membrane thickness, D_G is gas diffusivity, R is gas constant, T is temperature, P is permeability, δ_D is dense layer thickness and ε is porosity. According to the theoretical description, in order to minimize the effect of the membrane on the mass transfer resistance, the dense layer coating must possess a high CO_2 permeability and must be as thin as possible. Furthermore, according to the description of the mass transfer resistance in the porous material, it is easy to understand that in case of pore wetting the membrane resistance can increase significantly, as the gas diffusion in a liquid phase is 2 – 3 orders of magnitude lower than in a gaseous phase. A pore wetting of 2% can contribute to an increase of the membrane resistance that can represent up to 60% of the overall mass transfer resistance [26].

2.2 Composite Membrane

Since the mass transport rate has inverse relationship to the thickness of membrane, in order to have membrane with high gas permeance, the thickness of the dense layer should be as thin as possible. For this reason, thin composite membrane has been developed, with a thin dense layer on the top of a porous support. The first layer is able to ensure the separation performance of the membrane, whereas the porous layer is used as support, able to give mechanical strength to the system [27]. The depiction of composite membrane is given in Figure 5.
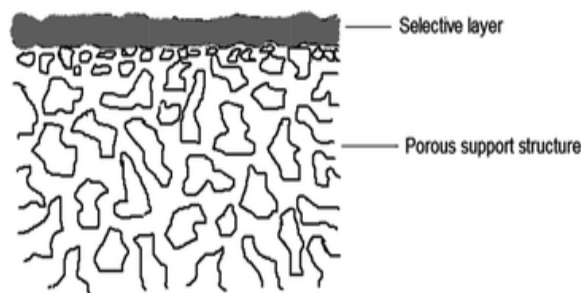
Figure 5: Depiction of composite membrane [28]

This can be obtained as asymmetric membranes or dip coating technique. For getting thin dense top layer dip coating is a useful technique. Composite membranes obtained by this method are often used in gas separation and pervaporation. In this method, flat sheet or hollow fiber is

immersed in dense polymer solution. The concentration of solution is usually 1 weight % solute/solvent. After removal from the bath, the membrane is placed in oven to remove any solvent. As a result of high temperature in oven, cross-linking occurs between porous structure and dense layer and it leads to adhesion of coated layer on porous sublayer. The illustration of dip coating is shown in Figure 6.
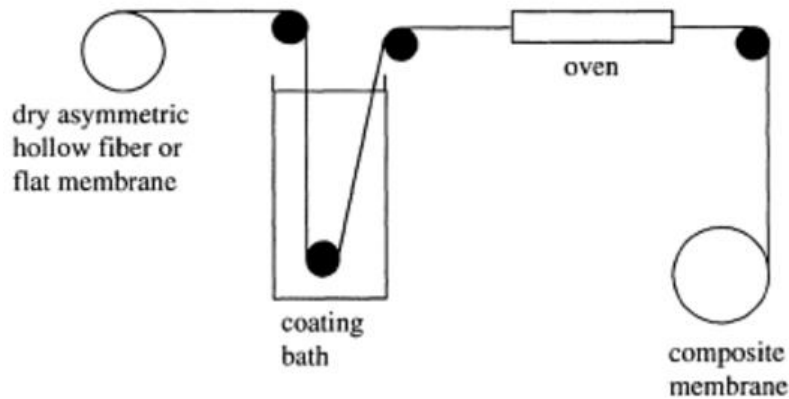
Figure 6: Illustration of Dip coating technique [29]

Four important parameters need consideration during dip coating.

- Polymer type and state (glassy or rubbery)
- Solvent characteristics
- Concentration of solution
- Molecular weight

The solvent selection has an effect on the coil dimensions. In good solvent, coils have large dimensions and vice versa. In poor solvents, coils aggregate and precipitation might occur. There is also a direct relationship between the molecular weight and coil dimensions. The state of polymer also plays important role in getting defect free thin layer [29].

As discussed in the previous section, adding a thin dense layer would contribute to mass transport resistance. A literature study showed that to compete with porous membrane contactor, the mass transfer coefficient of the thin dense layer in a composite membrane should be larger than 10^{-4} m/s [25]. It is also evident from **Figure 7** that dense membranes with CO_2 permeability of more than 100 Barrer are required for a thickness of the coating layer up to 1 μm, which is supposed to be a reasonable value.
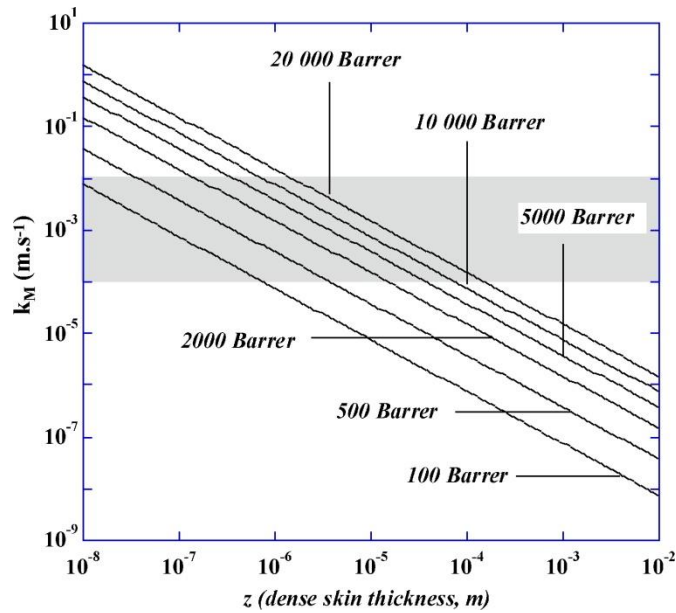
Figure 7: Dense layer thickness versus mass transfer coefficient [25]

2.3 Mass Transfer through Membranes

Generally, polymeric membranes are classified as microporous and dense membranes. In gas separation application, the porous membrane has little to do with separation and selectivity of species. As, in the porous membrane contactor, they only act as a barrier between 2 phases. The mass transport through a nonporous membrane is driven by pressure and concentration difference across the two membrane surfaces and the transport rate of each component is determined by its solubility and diffusivity across the membrane layer. Polymeric membranes can also be separated into two categories: rubbery and glassy membranes [27]. In glassy polymer, steric hindrance limits the free movement of polymer chains, attributing larger selective features. On the other side, in case of rubbery polymers, the segments in the backbone can easily rotate around its axis that result in higher permeation rates. When the temperature of glassy polymer is increased, thermal energy is sufficient to overcome steric hindrance and polymeric material changes from glassy to rubbery polymer [27].

The most typically used membranes for gas separation are dense polymeric membrane. In gas separation both types of porous and dense membrane work on different principles of in terms of transport mechanism. Generally, in industry porous membrane is used as support for structural support purposes. The transport through dense membranes can be described with the solution-diffusion mechanism, whereas in case of porous membranes three different

12

mechanisms can be identified: Knudsen diffusion, molecular sieving, and selective surface flow [2]. The diffusion mechanisms in porous membrane are shown in **Figure 8**.
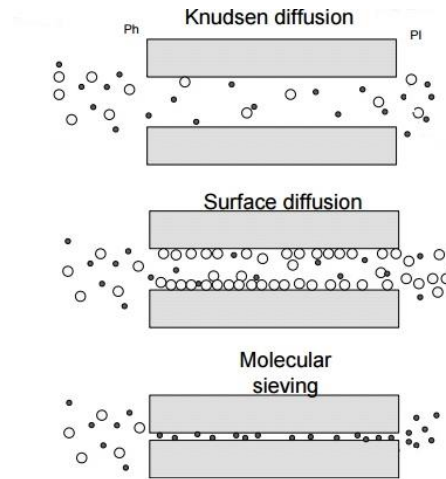
Figure 8: Diffusion mechanisms in porous membrane (Reprinted from [30])

In dense membranes, separation takes place by solution-diffusion mechanism [1]. The mechanism is a three-step process. The first step is the adsorption of gas molecules on the upstream side of membrane. Then, diffusion of molecules through the polymeric matrix takes place. Finally, the molecules are desorbed on the downstream of the membrane. The separation is carried out according to the kinetic or thermodynamic properties of the penetrants. In particular, the kinetic properties, such as the kinetic diameters, affect the diffusion of the penetrant within the polymer matrix, whereas the thermodynamic features, such as the critical temperature, affect the penetrant solubility within the membrane.

The mobility of the chains affects the polymer matrix for both rubber and glass polymers. The differences is that glasses are frozen in non-equilibrium state, which increases their equilibrium free volume, allowing to achieve larger transmembrane flux. Whereas rubbers are characterized by thermodynamic equilibrium and larger mobility of the polymer chains. For this reason rubbers are normally giving larger permeability and lower selectivity compared to glasses.

Solution-diffusion model is applicable to pervaporation, reverse osmosis and gas separation processes. In the solution-diffusion model, the permeability through a dense membrane can be described in terms of diffusion (D) and solubility (S)

$$P = D * S$$

The Fick's law provides mass flux and the flux is defined as the volume flowing through the membrane per unit area per unit time. It is also called permeation rate.

$$J_A = -D_A \frac{dc_A}{dx}$$

Where j_A = flux (mol/m^2.s), D_A = diffusion coefficient (m^2/s), $\frac{dc_A}{dx}$ = concentration gradient (mol/m).

Solubility (S) coefficient expresses the thermodynamic partitioning parameter and can be expressed as:

$$S_A = \frac{c_A}{p_A}$$

Where c_A is the concentration in the membrane phase (m^3 (STP)/m^3), p_A is the partial pressure of the component (bar) and S_A is solubility coefficient (m^3 (STP)/m^{3}bar). The combination of above equations would result in the following:

$$J_A = -D_A S_A \frac{dp_A}{dx} = P_A \frac{(p_{F,A} - p_{P,A})}{l}$$

Where P_A is the permeability coefficient of the penetrant A, l is membrane thickness, $p_{F,A}$ is partial pressure of component in the upstream (feed) side and $p_{P,A}$ is in the downstream (permeate) side of the membrane [27].

Ideally, the membrane selectivity can be written in terms of relative permeability rates of two or more components through the membranes. In attempt to increase permeability results in reduction of selectivity and vice versa. The performance is a trade of between the selectivity and permeability.

$$\alpha_{A/B} = \frac{P_A}{P_B}$$

The selectivity equation can be written in terms of diffusivity and solubility.

$$\alpha_{A/B} = \frac{P_A}{P_B} = \frac{D_A}{D_B} \cdot \frac{S_A}{S_B}$$

The diffusion coefficient (D) is a kinetic parameter that indicates the transport rate of penetrant in the membrane. The solubility (S) coefficient is a thermodynamic parameter and describes the amount of penetrant adsorbed into the membrane when in equilibrium with a given gas phase. Diffusion and solubility coefficients are temperature dependent, and this dependence can be expressed in terms of Arrhenius equation:

14

$$D = D_0 e^{\frac{-E_d}{RT}}$$

$$S = S_0 e^{\frac{-\Delta H_s}{RT}}$$

Where D_o and S_0 are pre-exponential constants, E_d activation energy of the diffusion, H_s is heat of solution, R is gas constant and T is temperature.

In view of the solution diffusion mechanism, the temperature dependence of gas permeation can also be given by Arrhenius relationship [31] and the activation energy of permeation, E_P, is obtained by adding E_d and H_s

$$P = P_o exp\left(\frac{-E_p}{RT}\right)$$

$$E_p = E_d + \Delta H_s$$

E_p gives information about free volume and size of gap between chain segments.
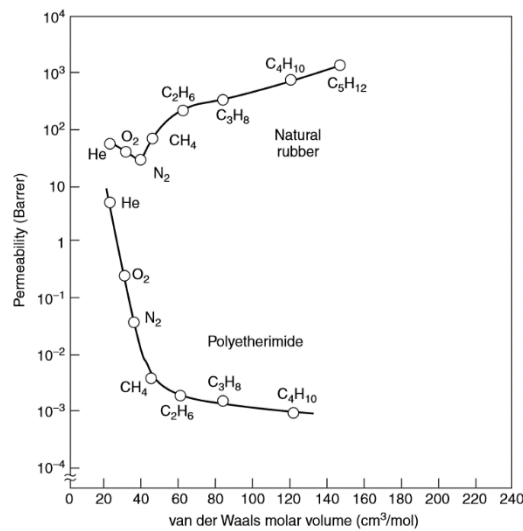
Figure 9: Permeabilities of glassy and rubbery polymer [27]

Figure 9 illustrates that the permeabilites of same components is different in case of glassy and rubbery polymers. In case of rubbery polymer, the permeability increase with increase in Van der Waals volume and follow opposite trend in glassy polymers.

Comparison of **Figure 9** with **Figure 10** explains that the kinetic size of penetrant affects the diffusion coefficient. The selectivity based upon diffusion is prominent in glassy polymer and solubility based selectivity dominant in rubbery polymers.
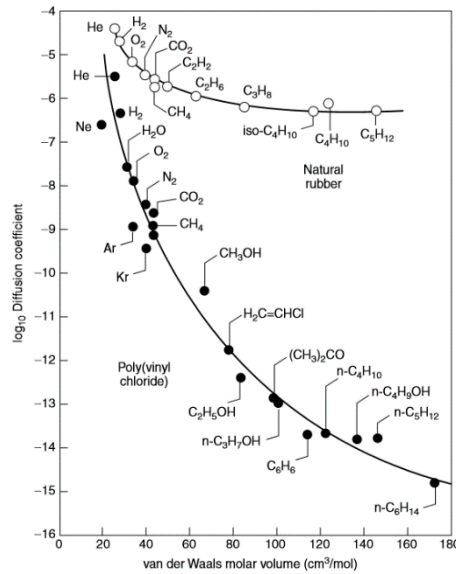
Figure 10: Diffusion coefficient in natural rubber (25° C) and PVC (30° C) [27]

2.4 Mixed Matrix Membranes

The use of inorganic membrane is also a viable option for gas separation purposes due to high flux and selectivity [32]. The inorganic membrane separation characteristics are well beyond Robeson upper bound limit [33] [32]. Unlike polymeric membranes, the inorganic membranes have some issues like brittleness, a high cost of production and inability to get a defect free surface. Hence, in mid-1980, the idea of mixed matrix membrane (MMM) started to be investigated as they combine the mechanical strength of organic membrane and separation ability of inorganic membranes [32]. The incorporation of inorganic phase, mostly nanosized, into polymer membrane resulted in mixed matrix membrane (MMM) with enhanced properties [34]. The schematic diagram of MMM is shown in Figure 11.
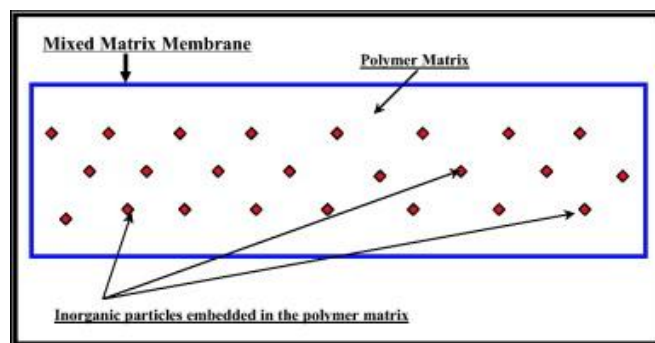
Figure 11: A depiction of mixed matrix membrane [35]

16

The inorganic dispersed phase has particular structure, surface chemistry and strength. Besides, so many factors like particle size, particle dispersion and particle structure, the polymer type can also play an important role in defining MMM properties.

The transport through mixed matrix membrane depends upon the final morphology of obtained mixed matrix membrane. **Figure 12** shows the possible morphology configuration that can be achieved upon embedding nanoparticles in a polymeric phase.
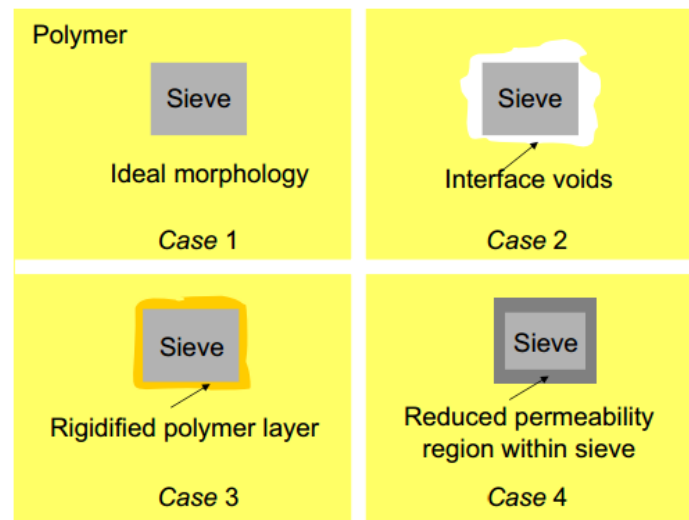
Figure 12: Morphology of MMM

Case 1 represents the ideal case morphological structure. In this case, the polymer phase is able to perfectly adhere to the surface of the inorganic phase, so that no discontinuities are faced by the penetrant along the transport through the membrane matrix. This configuration would correspond to the best one achievable for the MMM. Barrer and James [36] studied polymer/zeolite matrix and concluded that adhesion problems occur at polymer and inorganic phase interface (Case 2). This can result in larger permeability but lower selectivity, as gas molecules will go through non selective domains when they come closer to the inorganic phase [37], [38]. Duval suggested [37] that during classical casting technique solvent evaporation cause stress on MMM and results in the interface void morphology.

Li et al. [39] postulated that possible explanation of this could be different coefficients of expansion of inorganic and polymeric phase. Case 3 corresponds to chain rigidification, related to possible interactions between the polymer and the inorganic phase. Moaddeb and Koros [40] studied different high performance polymers with inclusion of silica particles and found out

that rigidified MMM can results up to 56% increase in O_2/N_2 selectivity due to low chain mobility. Consequently, increase in the selectivity near rigidified interface may be due to decrease in permeability.

Case 4 indicated a situation, in which porous inorganic fillers pores could be partially or completely filled by the polymer chains. Clariza et al. [41] reported that different porous fillers interact differently with polymer matrix. In case of NaX zeolite, the permeability of all the gases studied became lower because PDMS chains filled up the pores.

Table 3: Comparison of different membranes [42]

Properties	Polymeric membrane	Inorganic Membrane	Mixed Matrix Mem.
Cost	Economical	High cost	Moderate
Chemical & thermal stability	Moderate	High	High
Mechanical Strength	Good	Poor	Excellent
Compatibility to solvent	Limited	Wide range	Limited
Swelling	Frequently occur	Free of swelling	Free of swelling
Separation performance	Moderate	Moderate	Exceed upper limit
Handling	Robust	Brittle	Robust

The notable porous and non-porous nano-fillers are silica gel, carbon molecular sieve (CMS), zeolites, carbon nanotubes (CNT), metal oxides and MOFs [43]. Recently, graphene has received lot of attention due to its high mechanical characteristics and chemical stability [44].

Olivieri et al. [45] investigated the ageing effect of PTMSP with inclusion of two different grade graphene(M60 & IND G) and one graphene oxide (GO). It was concluded that graphene M60 and GO nanoparticles reduce the ageing time of PTMSP by modifying the relaxation time of polymeric chains, which would results in higher permeability.

Present-day investigations demonstrated that metal organic frameworks (MOFs) are promising materials for separation mechanism [46]. Zeolitic imidazolate framework (ZIF) is a subcategory of metal organic framework. Park et al. [47] synthesized twelve ZIFs and found that ZIF-8 and ZIF-11 possess small apertures suitable for gases and vapors separation. The study of gas adsorption further showed that they have high thermal stability and chemically resistance to organic solvents. The structure of ZIF-8 depicted in Figure 13.

18
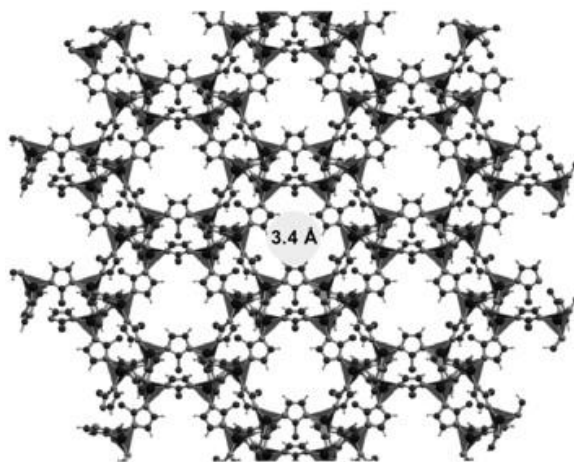
Figure 13: The structure of ZIF-8 [48]

C. Ordonez et al. [49] reported increase in permeability for Matrimid/ZIF-8 mixed matrix membrane for various single gases and gas mixtures. The permeability increase up to loading of 40% and show a sudden decrease in permeability at loading of 50 and 60%. It was concluded that this behavior might be due to ZIF-8 controlled gas transport instead of polymer based. The increase in ideal selectivities (CO_2/CH_4, H_2/CH_4) at higher loading of particles was also reported, suggesting ZIF-8 particles shows selective transport of gas molecules with smaller kinetic diameters [49].

Nafisi et al. [50] studied gas permeation with 6FDA-durene amine synthesized polymer & ZIF-8 as filler. It was reported that SEM results showed homogenous dispersion was achieved and with increase in the loading of particles, CO_2 permeability increased from 1468 to 2185 Barrer at 30% loading. However, increase in the loading lead to a decrease in CO_2/N_2 & CO_2/CH_4 selectivity, most likely related to the formation of interface voids in the membrane matrix.

Murali et al. [51] investigated the separation properties of MMMs composed of multiwall CNTs in Pebax-1657 at loading of 0-5% and TDI (2, 4-toluylene diisocyanate) was used for crosslinking. The CO_2 permeability and CO_2/N_2 selectivity (83.2 to 162) increased for crosslinked 2% CNTs-Pebax mixed membrane matrix. The initial attempts to successfully embed carbon molecular sieve (CMS) into polymeric membranes failed due to their porous rigid structure and interface voids [52]. Vu et al. [53] performed the most notable work on embedding CMSs into polymeric matrix. Ultem and Matrimid MMM with different loading of CMSs showed up to 45% increase in CO_2/CH_4 selectivity.

3 Experimental

3.1 Materials

Teflon AF 2400 (DuPont), Graphene and RGO (GNext), Electronic liquid FC-72 (3M), 2-(Diethylamino) ethanol (DEEA) (Sigma-Aldrich 99% pure), 3-(Methylamino) propylamine (MAPA) (Sigma-Aldrich 98% pure), ZIF-8 (Basolite Z1200) (Sigma-Alrich).

3.1.1 Membrane preparation

Teflon AF 2400 is a glassy amorphous copolymer with transition temperature 240 °C. The chemical composition of AF2400 is 87 mol% 2, 2-bistrifluoromethyl- 4, 5-difluoro-1, 3-dioxole and 13 mol% tetrafluoroethylene.

The dense self-standing membranes of Teflon AF 2400 were prepared by using 1 wt. % of polymer in FC-72 solvent (boiling point = 56 °C) [31], [54]. The solution was stirred magnetically over night to completely dissolve the polymer. Afterwards, the solution was casted on glass petri dish and air dried overnight under ambient temperature. The membrane samples were removed using a doctor blade and water and dried in oven at 200°C under vacuum conditions. This pre-treatment of the membrane is believed to be able to completely remove the residual solvent from the matrix, considering the boiling point of the solvent.

Mixed matrix membranes of Teflon AF2400 were prepared with different concentrations of reduced graphene oxide (RGO) or ZIF-8 (zeolite imidazolate framework) as self-standing samples. Firstly, the nanoparticles were sonicated in solvent for 4-5 hours in an ultrasonic bath (VWR). The temperature of the tub is kept below 40°C, by frequent changes of the water bath. The weight of flask was calculated before and after sonication in order to calculate the solvent loss. The lost amount of solvent was then added to solution. Afterwards, a certain polymer amount was added to the mixture and magnetically stirred over night to dissolve the polymer. The polymer solution containing nanoparticles was again sonicated at same conditions. The solution was casted on glass petri dish and dried overnight under a fume hood at ambient temperature. Subsequently, the membranes were dried at 200°C in oven under vacuum condition overnight. The procedure for the preparation of MMM depicted in **Figure 14**.
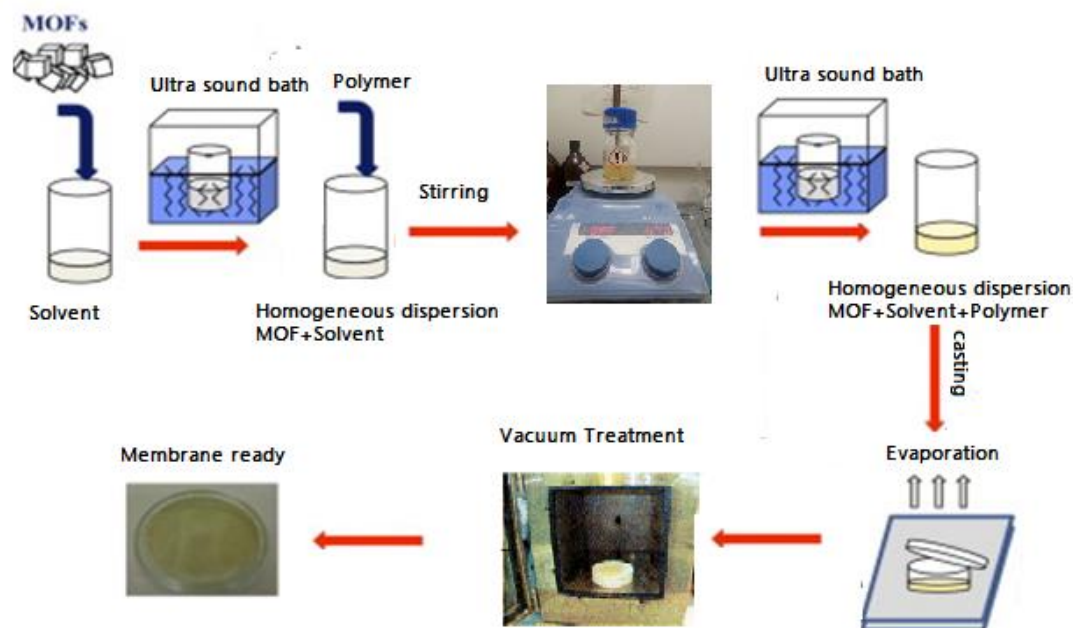
Figure 14: Illustration of MMM manufacturing process [55]

3.2 Characterization Techniques

3.2.1 Single Gas permeation

The gas permeability was measured in a single gas permeation setup, through a constant volume variable pressure method. The system measures permeate flux by monitoring pressure difference across the membrane cell with the help of pressure transducer. In addition, the rig is placed in a cabinet with a temperature control, so that experiments up to 60°C can be carried out. The downstream volume has been preventively calibrated, and the procedure is reported in Appendix C.

A permeation area of 2.2 cm^2 was used. The sample thickness was measured using digital micrometer (Mitutoyo corp., Japan). The sample was exposed to vacuum overnight to ensure complete removal of any dissolved penetrant in the polymer matrix. Subsequently, a leak test was performed to investigate the leaking rate, by closing downstream side valve and keeping the upstream exposed to vacuum for two hours.

The high-pressure vessel (shown in Figure 15) was filled with feed gas by opening valve 01 and the vacuum pump was turned off and valve 06 was closed. The upstream valve 03 was opened and gas was introduced into the system. Sudden decrease in pressure was observed on the upstream side, which is due to tubing volume. The increase in downstream side was measured with the help of pressure transducer (WIKA). The signals from transducer were

22

digitalized and received as pressure in Lab view 7.1. The data was analyzed using Microsoft Excel and the slope was calculated after regular intervals to find steady state condition. The effective pressure difference was maintained between the upstream and downstream side of membrane. Permeability is steady state flux normalized with pressure difference and thickness. The Figure 16 describes the variation of pressure with time and the consequent dependence of the flux with time.
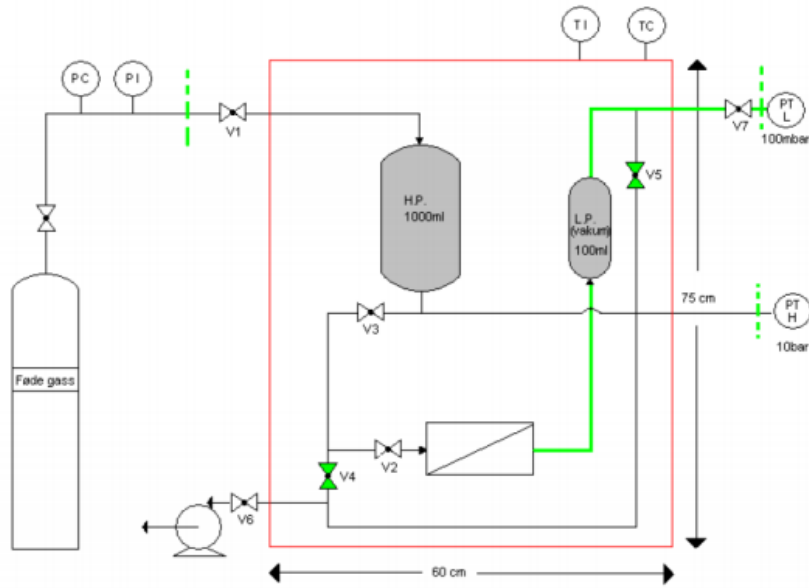
Figure 15: Single Gas Permeation Setup
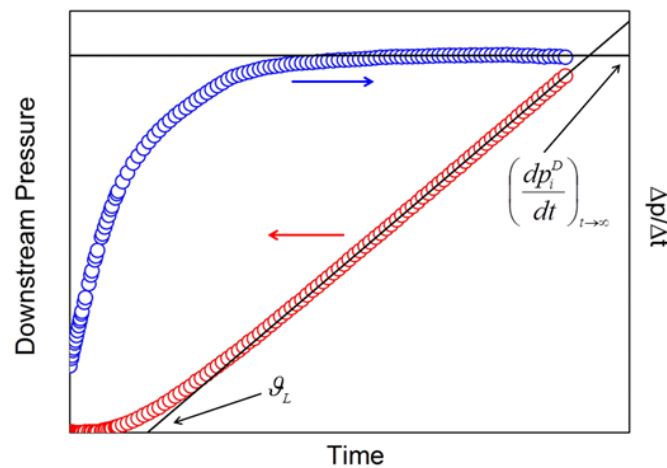
Figure 16: Variation of downstream pressure and transmembrane flux over time obtained from the single gas permeation setup (reprinted from ref. [56])

The permeability can be calculated from the following equation when steady state conditions (dp/dt is constant) are reached as:

$$P_A = \frac{V_d l}{\Delta p A R T}\left[\frac{dp}{dt} - \left(\frac{dp}{dt}\right)_{leak}\right]$$

Where P is gas permeability (1 Barrer = 10^{-10} cm^3 (STP) cm cm^{-2} s^{-1} cmHg^{-1}), l is membrane thickness, Δp is the pressure difference between upstream and downstream pressure, V_d is downstream volume, A is membrane area, $\frac{dp}{dt}$ is the transmembrane flux, , $\left(\frac{dp}{dt}\right)_{leak}$ is the term related to the possible leakage R is real gas constant and T is the temperature.

The experiment was carried out at different temperatures (RT, 40 and 60°C) for CO_2, N_2 and O_2. The membranes that have been used for gas permeation were Teflon AF 2400 and graphene, RGO, and ZIF-8 mixed matrix membranes. The tests for MMM were done for CO_2 and N_2. Even though N_2 was not relevant for the membrane contactor investigation, the N_2 permeability tests were carried out in order to better understand the effect of the nanoparticles dispersion within the matrix on the selective features of the obtained membranes.

3.2.2 Pervaporation

The pervaporation experiments have been performed using the apparatus shown in Figure 17. The membrane was placed inside the sample holder, which had a permeating area of 35.8 cm^2. The pervaporation experiments were carried out in the temperature range 40 to 60 °C. To avoid concentration polarization the flow of the system was kept at a value larger than 50 ml/min, as this value is already much larger than the real one obtained through the membrane.

The feed was pumped from 1-liter reservoir and preheated before entering into the membrane module. An initial step was performed before every series of experiments exposing the membrane to the real experimental conditions (liquid on the feed side, vacuum on the permeate side) overnight, making sure the achievement of steady state conditions. During the experiments, the cold sampling trap was immersed into liquid nitrogen (T ≈ -170 °C) for 4 - 8 h to collect permeate as shown in **Figure 17**. The permeate pressure was kept constant at a value of 2.5-3.5 mbar during experiments. Every single data point is obtained as average of at least three consecutive flux measurements that are able to show a constant flux. Between every experiment, the membrane was continuously exposed to the experimental conditions previously mentioned (liquid on the feed side, vacuum on the permeate side).

24

The amount of sample-permeated trough the membrane and trapped in the cold trap was measured by a Mettler Toledo scale with a precision of 0.1 mg, and subsequently the overall flux has been calculated according to the following formula:

$$J = \frac{w}{A\,t}$$

Where w is weight of permeate sample in grams, A is membrane active surface area in cm^2 and t is time in hours.

When amine mixtures were considered as feed solutions, permeate and feed samples were collected and analyzed through IC analysis in order to find the amine concentration, which allows calculating the single amine flux at the given feed composition (IC analysis were performed by Dr. Luca Ansaloni).
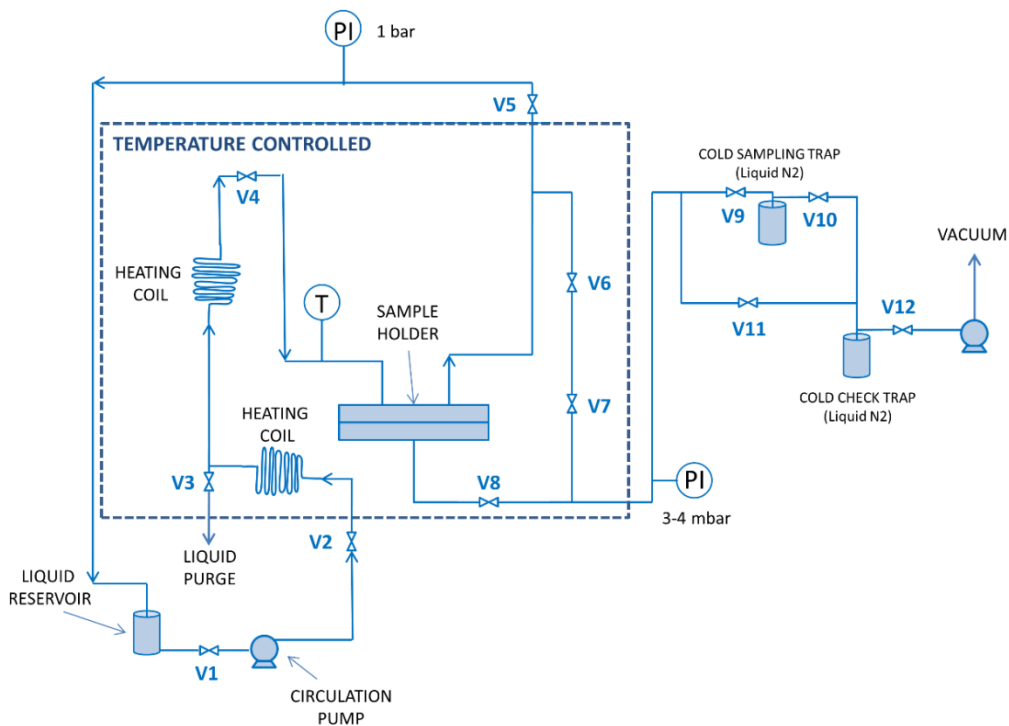
Figure 17: Pervaporation setup (reprinted from ref [11])

3.2.3 Morphological Characterization

The resolving power of eye is 0.01cm and to observe smaller entities a microscope is needed. The microscope can be optical or electronic. The scanning electron microscope is a device that sweeps surface with a finely focused electron beam in a vacuum, detect the data delivered from the specimen and presents an extended picture of the example.
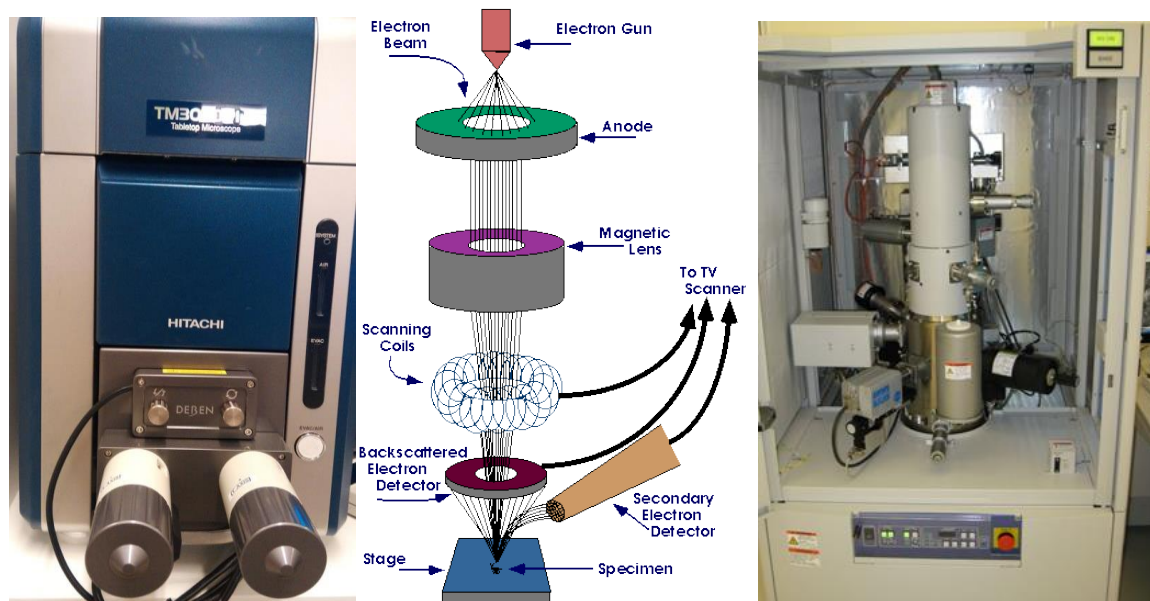
Figure 18: Scanning Electron Microscope: TM3030PLUS (left picture), working mechanism (central picture), S(T)EM 5500 (right picture).

When electron beam strikes the samples, different signals are generated. The scanning electron microscope utilizes the secondary electrons to generate a topographical structure of the sample. To increase the electric conductance and to avoid damage to the sample, the material was sputtered with a thin layer of gold or platinum/palladium. The working of scanning electron microscope is shown in **Figure 18**.

The morphology of MMM membranes was studied with the SEM TM3030PLUS and S(T)EM 5500 from HITACHI and sputtering coater Q150R from Quorum. The S(T)EM 5500 is in-lens microscope which can achieve resolution up to 0.4nm and EDX-system gives 10 times better collection efficiency of X-rays as compare to regular SEM. The samples were attach to specimen stub with the help of conductive tape and was placed in sputtering device. The samples were coated with gold of 5nm thickness for TM3300 and coated with platinum/palladium of 5nm thickness for S(T)EM 5500. The samples were removed and the specimen stub was attached to holder in microscope. The system was evacuated with the help of vacuum pump.

3.2.4 **Pressure Decay Rig**

Vapor sorption experiments were performed using pressure decay rig, whose layout is depicted in Figure **19**. Before the experiment, the sample was exposed to vacuum overnight to remove any possible penetrant left in the polymer matrix. A LN_2 cold trap was used in upstream of

vacuum pump to avoid any vapor condensation and contamination in pump. A vacuum test was performed to investigate the leak rate.

A copper wire was carefully wrapped around the membranes to avoid the membrane surface from touching the sample holder wall, which would lead to error in absorption calculations. The liquid containers, used to produce the vapor and the vacuum pump were connected through stainless steel tubing and valves. Moreover, at every connection, VCR fittings and metal gaskets were used to ensure a high vacuum grade of the system. The liquid was stored in 150 ml container and vaporized at desired temperature in the pre-chamber, (shown in **Figure 19**) which is connected to pressure sensor.
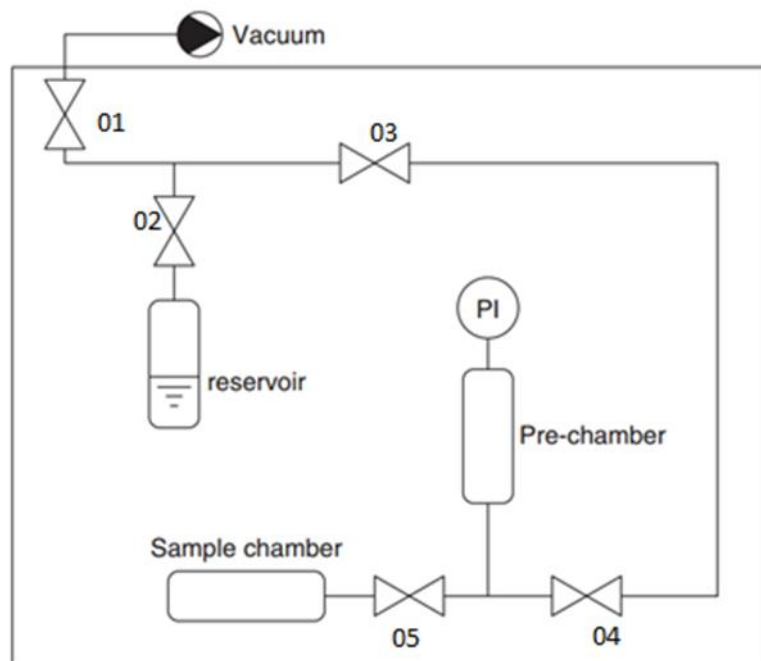
Figure 19: Depiction of pressure decay rig (reprinetd from ref [34])

After a leak check, the vacuum pump and valve V01 were closed and simultaneously valves V2 and V03 were opened. The valve V04 was carefully opened to attain certain vapor pressure in pre-chamber. Once the system achieved a steady value of the pressure, the valve towards the sample chamber was opened. At first, the pressure value was suddenly decreased which is due to expansion. After some time, depending upon kinetics of penetrant, the value remains constant for all penetrants.

The decrease in pressure was measured with the help of pressure transducer (MKS, Barotron), with a full scale of 10 and 100 mbar. The signals from transducer were digitalized and received

as pressure in Lab View 7.1. The data was analyzed using Microsoft Excel and the calculation done after regular intervals to find steady state condition. Fickian sorption kinetics solution was proposed by Crank [57] by fitting of experimental data. **Figure 20** illustrates the typical output of sorption experiment. The diffusion can be directly estimated for a given pressure jump and the solubility can be directly estimated from the equation given below.

$$\frac{M_i(t)}{M_{i,\infty}} = 1 - \sum_{n=0}^{\infty} \frac{8}{(2n+1)^2 \, \pi^2} \exp\left[-D_i \frac{(2n+1)^2 \, \pi^2 \, t}{4\delta^2}\right]$$

Where M_i is initial mass and $M_{i,\infty}$ is final equilibrium mass of the sample.
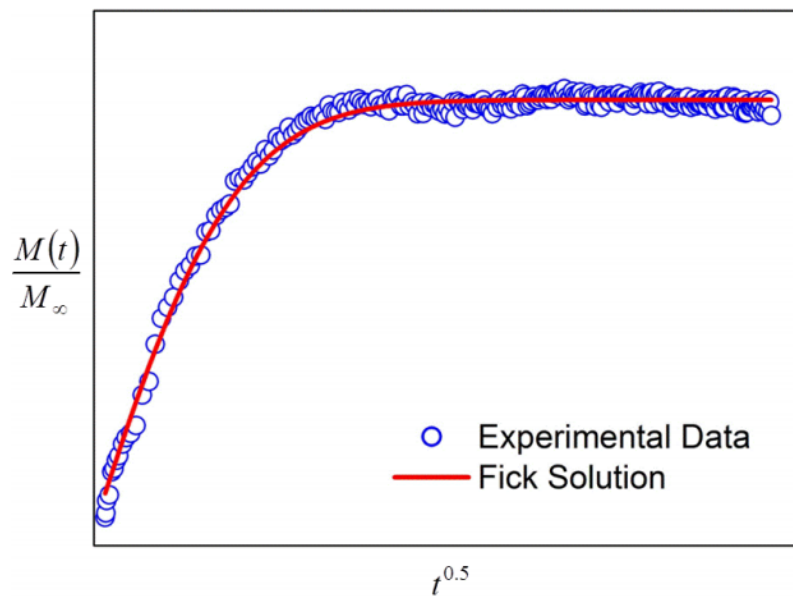
Figure 20: Sorption experiment typical output [56]

The sorption isotherm is usually obtained by incremental steps, by increasing pressure in each step to a certain point.

4 Results and Discussion

4.1 Morphological Characterization

The self-standing MMMs with different concentrations of ZIF-8 and RGO were prepared. The samples were fractured in liquid nitrogen to avoid any damage to cross-section. The SEM image of cross section of ZIF-8 MMM with 10% loading is shown in **Figure 21**.
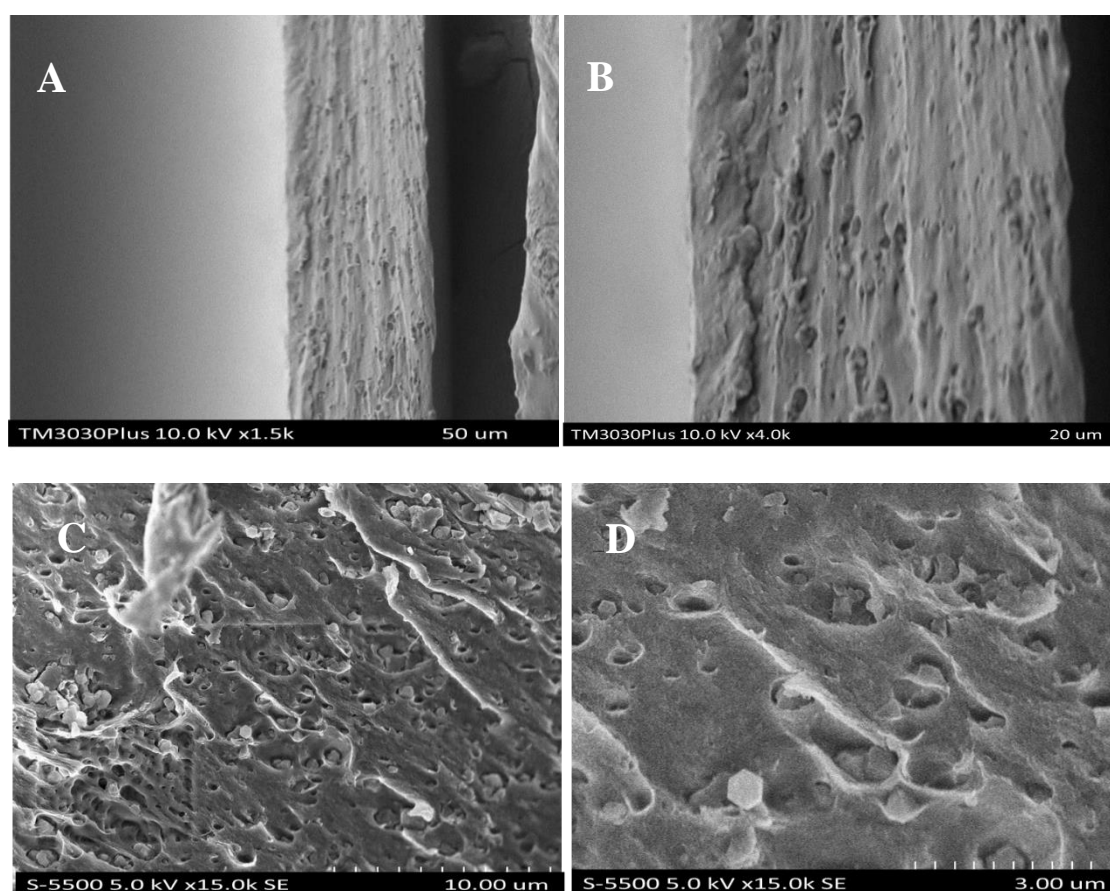
Figure 21: SEM images of 10 wt% ZIF-8 MMM

(A and B: cross section images obtained from TM3030 Plus; C and D: cross section images obtained from S(T)EM)

Firstly, the results of the membrane morphology studied with Hitachi TM3030lus are shown in A and B. The membrane appeared to have good morphology with uniform dispersion of particles as the ideal case 1 shown in **Figure 12**. To further characterize and study the morphology in detail, S(T)EM S5500 was utilized, as it allows to reach a better resolution at high magnification. The membrane cross section results are shown in C and D. When observed closely, the membrane morphology appeared to be 3-phased MMM, more similar to the case 2

reported in the **Figure 12**. The voids are present in MMM, which suggests poor interaction between inorganic and polymer phases that can also explain the possible decrease in selectivity. Particle size of ZIF-8 particles in MMM calculated from SEM images are shown in **Figure 22**. Torad et al. [58] reported similar size for mono dispersed ZIF-8 particles. It was also reported that the middle-sized particles (300 nm) have an active surface area of 1570 m^2/g and pore volume 0.9 cm^3/g.
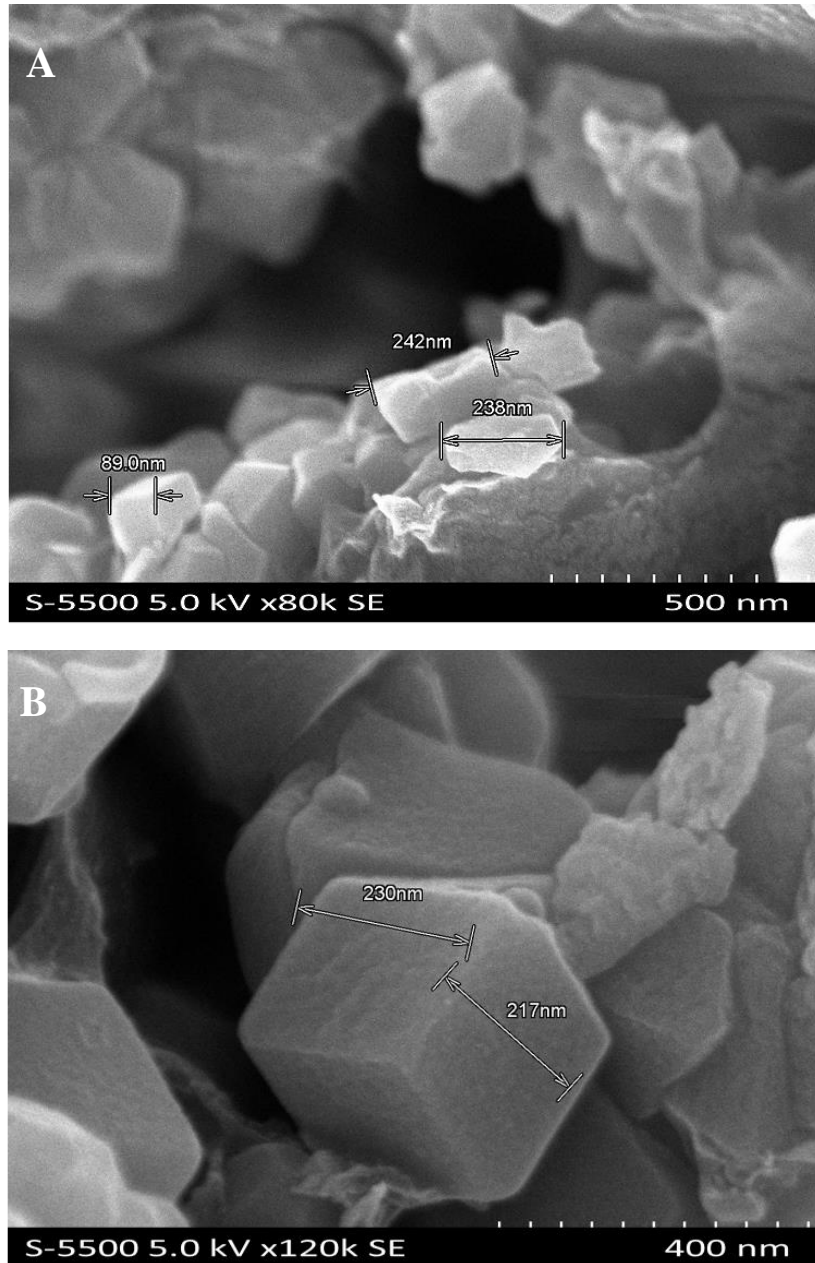
Figure 22: SEM images of ZIF-8 particles in MMM with sizes

High magnification SEM images of ZIF-8/Teflon AF2400 MMM with 7.5% loading are shown in **Figure 23**. At the loading of 7.5%, there were observable aggregate or clusters of dispersed phase. The image A is the cross section and image B is the surface of MMM. The sieve in cage morphology was not observed in the cross section of the membrane, which indicates good adhesion of inorganic and the organic phase in the membranes and dense membrane. To avoid damage to the samples, magnification was limited to 10 um. The damage to membrane is visible in **Figure 49**. The rough surface of membrane can be attributed fracture process during preparation.
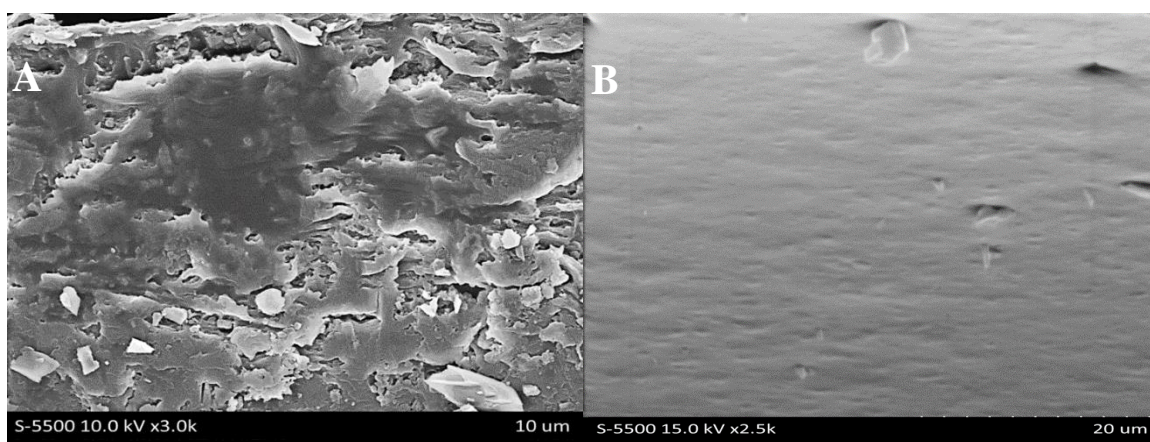
Figure 23: SEM images of 7.5 wt% ZIF-8 Teflon AF 2400 MMM
(A: Cross section and B: Surface morphology)

SEM images of 10%RGO/Teflon AF 2400 MMM are shown in **Figure 24**. The two images were taken from different parts of cross-section. The SEM results shows 10% RGO/Teflon AF2400 membrane is dense. However, there are few voidages visible in polymer matrix that might be due to RGO aggregation. The AFM analysis is needed to further study and characterize the membrane.
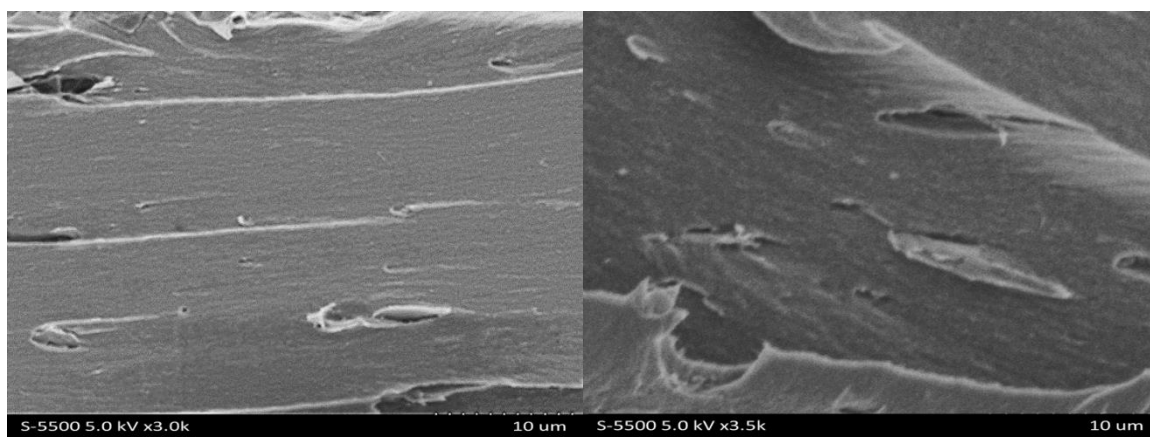
Figure 24: Cross section SEM images of 10% RGO-Teflon AF 2400 MMM

4.2 Gas permeation

4.2.1 Teflon AF2400

According to the initial compatibility study, glassy perfluoropolymers membranes showed good chemical, related mainly to the strength of the C-F bond [10]. In particular, the Teflon AF series, AF2400 and AF1600 (the chemical structure of Teflon AF membrane is given in **Figure 25**) showed good chemical stability with the 3rd generation solvents. According to the larger gas permeability reported in literature, Teflon AF2400 was chosen for further characterization.
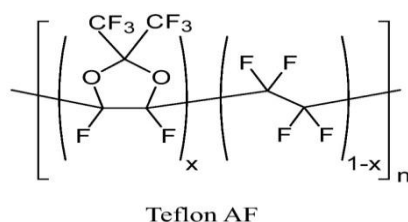
Figure 25: Structure of Teflon AF polymer series (AF 2400: x=0.87, AF 1600: x = 0.66)

Therefore, the permeability of different gases like oxygen, nitrogen and carbon dioxide were studied in the temperature range from 23 to 60 °C. **Table 4** reports permeability of pure gases at different temperatures. From the table, it can be seen that the permeability of the gaseous penetrants increases in the following order $N_2 < O_2 < CO_2$, following both the kinetic size ($N_2 > O_2 > CO_2$) of the penetrants and their condensability ($CO_2 > O_2 > N_2$). This is related to the fact that the diffusivity of gases is directly related to kinetic size. The kinetic size of CO_2 (3.3

32

Å) is lower than O_2 (3.46 Å) and N_2 (3.64 Å) [42] which can favor the diffusion coefficient of CO_2 to a larger extent compared to the other two gases. In addition also the gas condensability plays an important role, affecting the solubility coefficient. The critical temperature of CO_2 (31°C) is larger than the one of N_2 (-147°C) and O_2 (-119°C), resulting in a larger solubility of the first gas compared to the latter two ones [34].

Furthermore, a peculiar effect is observed in the gas permeability coefficient by changing the operative temperature (**Figure 26**). The CO_2 permeability at room temperature corresponds to 3145 Barrer and it decreases to 2870 Barrer at 40 °C and to 2615 Barrer at 60 °C, suggesting that the solubility coefficient has a larger influence on the gas permeability compared to the diffusion coefficient. However, in case of N_2 and O_2 an opposite behavior is observed. In case of N_2, permeability 565 Barrer at room temperature and increase to 642 Barrer at 40 °C and 682 Barrer at 60 C. Similarly, in case of O_2, the permeability 1180 Barrer at room temperature, 1225 Barrer and 1275 Barrer at 40 and 60 °C respectively . For both gases, the solubility is much lower compared to CO_2, thus their permeation relies more on their ability to diffuse across the matrix, which is positively affected by the temperature increase.

The permeability of gases in Teflon AF 2400 membrane is in good agreement with literature [59] [60], but slightly lower than what is reported in [31]. The selections of the solvent and casting technique have been reported to be contributing factors in this regard. It also has been reported that residual solvent can result in increased permeability and decreased selectivity [60].
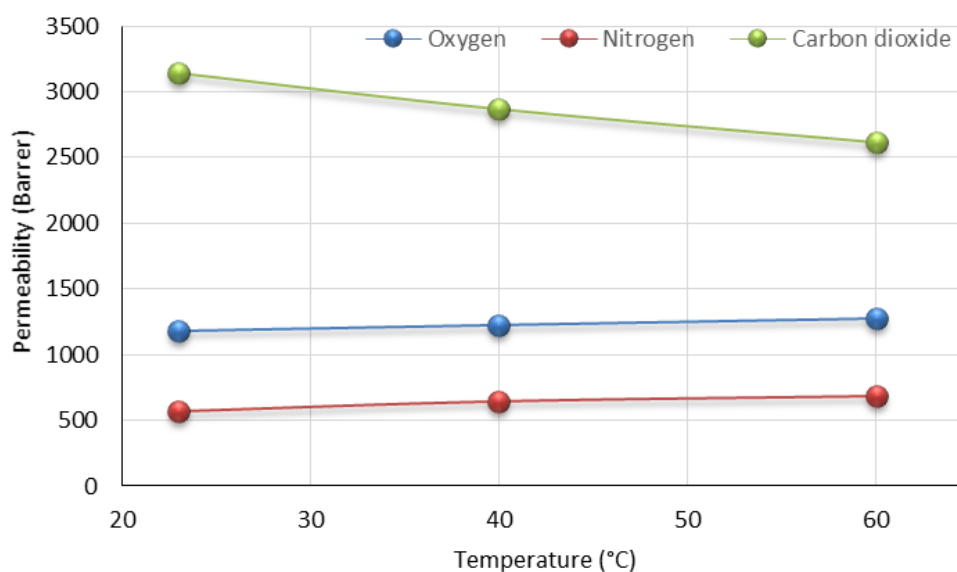
Figure 26: Gas permeability in Teflon AF 2400 at different temperatures (upstream pressure = 1.6 bar)

The CO_2/N_2 selectivity in Teflon AF 2400 membrane is 5.5 at room temperature and decrease with increase in temperature to 4.47 and 3.83 at 40 and 60 °C respectively. Similar trend was observed for CO_2/O_2, selectivity is 2.66 at room temperature, 2.34 and 2.05 at 40 and 60 °C respectively.

The temperature dependency of permeability in polymeric dense membrane can be usually explained by Arrhenius equation, reported in paragraph 2.3.

Table 5 shows the activation energy of permeation of CO_2, N_2 and O_2 in Teflon AF2400. In case of CO_2, a value equal to -4.1 kJ/mol is obtained, where the negative value is related to the fact that permeability is found to decrease at increasing temperature. In addition, this is slightly higher than the one reported in literature [31]. In case of N_2 and O_2, the activation energy of permeation is found to be equal to 4.09 and 1.176 kJ/mol respectively. In this case the value is positive, accordingly to the behavior previously mentioned in the description of effect of temperature on the permeability coefficient. Furthermore, the obtained data appeared to be different from the one observed in literature, which are -0.40 KJ/mol and -2.50 KJ/mol for N_2 and O_2 respectively. The detailed calculations are shown in Appendix D.

For typical glassy polymers, E_d increase and ΔH_s decrease with increase in temperature and overall permeability of gases increase also because $\frac{E_d}{\Delta H_S} > 1$. The increase in permeabilities for N_2 and O_2 clearly follow this trend but permeability of CO_2 decrease with increase in temperature. Pinnau et al. [31] and Masuda et al. [61] reported decrease in permeabilities for gases i.e. negative permeation energies ($E_d + \Delta H_s < 1, \frac{E_d}{H_S} < 1$) for high FFV polymers Teflon AF 2400 and PTMSP respectively. When temperature is increased the solubility of CO_2 is decreased which resulted in lower permeability.

<p align="center">Table 4: Pure gas Permeabilities of Teflon AF2400</p>

Temperature (°C)	Permeability (Barrer)			Selectivity	
	CO_2	N_2	O_2	CO_2/N_2	CO_2/O_2
23	3145	565	1180	5.56	2.66
40	2870	642	1225	4.47	2.34
60	2615	682	1275	3.83	2.05

4.2.2 **Teflon AF2400 mixed matrix membrane**

As discussed in the introduction, the core idea of the present work is to use nanoparticles in Teflon AF 2400 in order to achieve membrane with better selectivity towards 3rd generation solvents and possibly larger CO_2 permeability. Therefore, in pervious part of the project, graphene was considered as filler to produce MMM and tests were performed to investigate the influence of its inclusion on the gas permeability and selectivity of CO_2 versus other gases. The results showed that graphene change permeability from 3100 Barrer to 3200 Barrer, but selectivity with respect to N_2 was slightly decreased [10]. For this reason, this type of mixed matrix membrane has not been considered worth of further investigation. The results obtained for this type of MMMs are reported in Appendix E for the sake of completeness.

In this part of the project, the effect of reduced graphene oxide (RGO) and ZIF-8 nanoparticles dispersion on Teflon AF 2400 membrane permeability was studied. To the best of author's knowledge, no prior work was performed on Teflon AF 2400 mixed matrix membranes using ZIF-8 or graphene. The addition of RGO and ZIF-8 resulted in a remarkable increase of CO_2 and N_2 permeability. In case of ZIF-8, it is believed that the cage structure and the larger CO_2 affinity should be the main responsible for the increase of the CO_2 flux, but in case of RGO, it is most likely related to the creation of voids at the interface of nanoparticles and the polymer chains. At a 3% loading of ZIF-8, the CO_2 permeability found to be 3784 Barrer, with loading of 5% the permeability increased to 4074 Barrer and at the loadings of 7.5% and 10% the CO2 permeability increased to 4175 and 4256 Barrer respectively. However, the ZIF-8/Teflon AF 2400 at loading 10% MMM showed visible particles aggregation on the membrane surface, suggesting a possible concentration limit of the ZIF-8 in the AF2400 matrix. For this reason, the matrix obtained with 10 wt% ZIF-8 was not considered for further characterization.
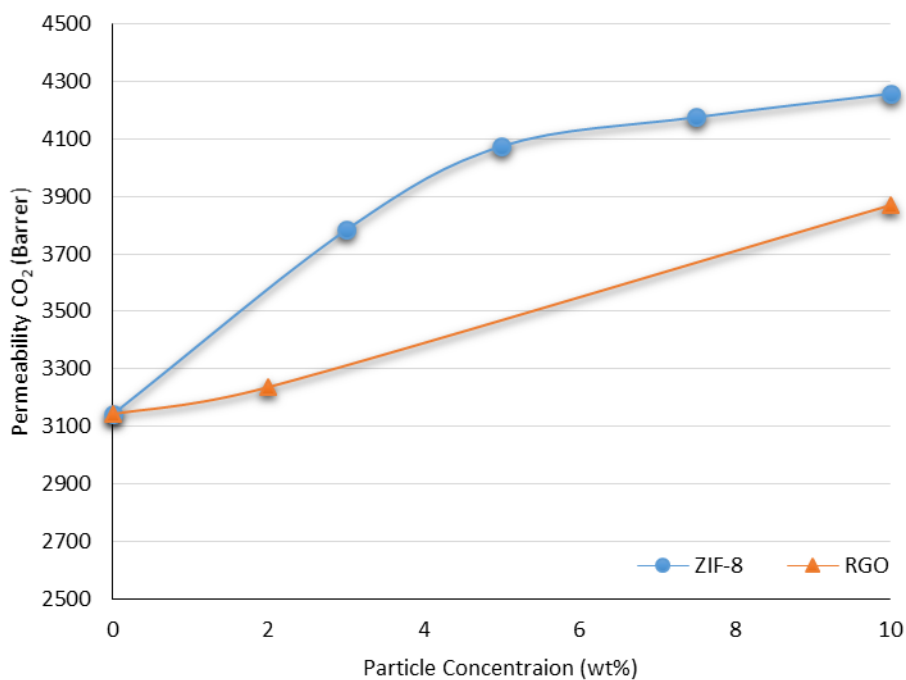
Figure 27: CO_2 permeability in Teflon AF2400 mixed matrix membranes obtained embedding different concentration of ZIF-8 and RGO.

In Teflon AF2400/RGO MMM at loading of 2%, the calculated CO_2 permeability was 3238 Barrer and with the loading of 10% RGO, the permeability was found to be 3869 Barrer. However, the 10% RGO/Teflon AF 2400 MMM showed an increase of the stiffness of the membrane layer, which became much more brittle.

The increase in permeability can also attributed to increase in the chain distance between polymer chains. It has been reported that, in MMM; nanoparticles interrupt the rigid and bulky chain structure leading to increase in permeability [62], [63]. The permeabilities for N_2 at different loadings of RGO and ZIF-8 in Teflon AF2400 at different temperatures were studied. The N_2 permeability seems to follow similar trend as CO_2 permeability, with increase in particle concentration have positive impact on permeability. In RGO MMM at the loading of 3%, the N_2 permeability was 627 Barrer and it reaches up to 798 Barrer at 10% loading. In case of ZIF-8 MMM, the N_2 permeability is 759 Barrer at 3% loading, at 5% 800 Barrer, at 7.5% 867 Barrer and finally 926 Barrer at 10% loading.
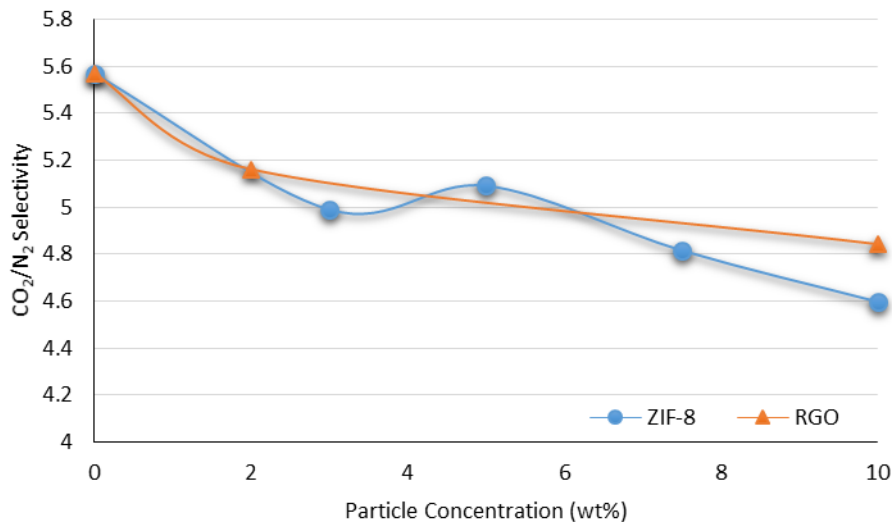
36

Figure 28: CO_2/N_2 Selectivity in Teflon AF2400 mixed matrix membranes obtained embedding different concentration of ZIF-8 and RGO.

Figure 28 illustrates the selectivity of CO_2/N_2 as a function of dispersion, the selectivity decrease from 5.6 to 4.7 with increase of the ZIF-8 nanoparticles dispersion in polymer matrix. This suggests that the formation of non-selective region (i.e., interface voids) occurred also in case of ZIF-8 dispersion. Similarly, the CO_2/N_2 selectivity for RGO MMM at the dispersion of 10% was reduced to 4.84. The following results was expected as disruption of bulky glassy structure does not contribute to selectivity. It is the formation of voids at the interface that reduce the selectivity as reported for different MMM [50], [34]. The overall performance of MMM can be rationalized with morphological characterization. All MMMs seems to have case 2 shown in **Figure 12**, the unselective voids resulted in increased permeability and decreased selectivity.

According to the results obtained, the 7.5 wt% ZIF-8 MMM was considered for further characterization. The effect of temperature on permeability and selectivity shown in **Figure 29** and **Figure 30**. The CO_2 permeability at room temperature corresponds to 4175 Barrer and it decreases to 3405 Barrer at 40 °C and to 3317 Barrer at 60 °C, suggesting that the solubility coefficient has a larger influence on the gas permeability compared to the diffusion coefficient. As discussed earlier, Arrhenius equation can describe the effect of temperature. The value of activation energies for 7.5% ZIF-8 MMM shown in **Table 5**. The trends of permeabilities for N_2 and CO_2 are similar as seen earlier for pure Teflon AF 2400 but drops in permeability for CO_2 at 40 °C is significant which might be due to experimental error. The N_2 permeability calculated at room temperature was 828 Barrer, 838 Barrer at 40 °C and 857 Barrer at 60 °C.
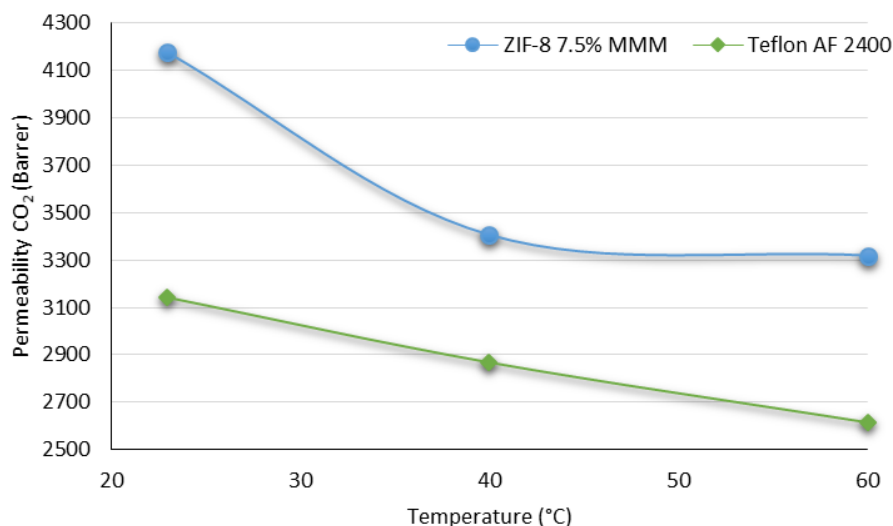
Figure 29: Permeabilitiy of CO_2 as a fuction of temperature in Teflon AF2400 and the MMM containing 7.5 wt% of ZIF-8.

The CO_2/N_2 selectivity in ZIF-8 7.5% MMM is illustrated in **Figure 30**. The selectivity is 5.04 at room temperature and decrease with increase in temperature to 4.06 and 3.87 at 40 and 60 °C respectively. The pure Teflon AF 2400 is more selective than nitrogen at every temperature than at 60 °C, where the ZIF-8 7.5% MMM is slightly more selective. The presence of dispersed particles restricted the free movement of polymeric chains and membrane at high temperature became selective.
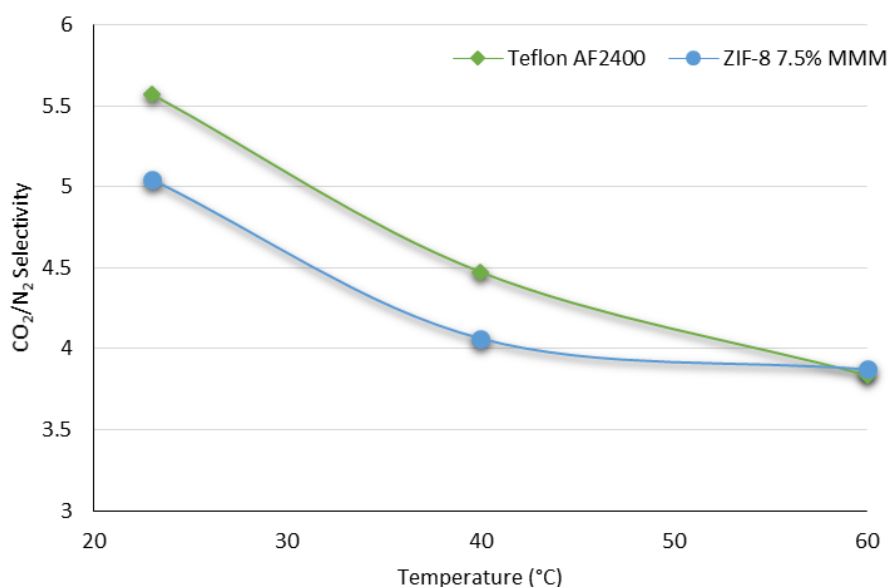
Figure 30: CO_2/N_2 selectivity as a fuction of temperature in Teflon AF2400 and the MMM containing 7.5 wt% of ZIF-8

Table 5: Activation energies of permeation for different polymers

Polymer	Activation energy of permeation, Ep (kJ/mol)		
	N_2	O_2	CO_2
Teflon AF2400 (this work)	+4.09	+1.716	-4.091
Teflon AF2400 7.5% (this work)	+0.763	----	-5.065
Teflon AF 2400 [31]	-0.400	-2.50	-6.7

Table 5 shows activation energies of CO_2 and N_2 in ZIF-8 7.5% MMM. The activation energy for CO_2 in MMM is lower than pure Teflon AF2400, the presence of ZIF-8 might have enhanced the solubulity of CO_2 in the matrix. In case of temperature shift, the difference inpermeability is more prominent, as the critical temperature of CO_2 is high, the solubility decrease in membrane is much higher. In case of CO_2, calculated value was -5.06 kJ/mol and for N_2 the activation energy equals to 0.763 kJ/mol. The activation energies are lower than the pure Teflon AF2400.

4.3 **Pervaporation**

In order to investigate the amine permeation through the membrane layer, pervaporation experiments were carried out in the temperature range 40 to 60 ± 0.5 °C for pure H_2O and 3D3M for MMM. The temperature range chosen according the best operating conditions suggested for the CO_2 absorption in the solvent [64].

In addition, pervaporation tests been carried out also on MEA aqueous solution at 60 °C containing, 50% and 70% MEA in pure Teflon AF2400. Indeed, one possible way to reduce the regeneration energy in absorption process is to reduce the water content in the absorbent. However, larger amine concentration in the liquid phase would correspond to larger amine evaporation in the absorption column, reaching values that are not tolerable in terms of emissions. Therefore, membrane contactor can offer a proper solution for the full exploitation of highly concentrated amine-based solvents.

The results related to the pervaporation tests for 3D3M through pure Teflon AF2400 are provided by Dr. Luca Ansaloni [11] and are simply used for comparison.

4.3.1 **3rd Generation solvents**

The flux of the different components of the 3D3M solution (H_2O, DEEA and MAPA) through pure Teflon AF2400 and the MMM obtained using ZIF-8 shown in **Figure 32**, **Figure 33** and **Figure 34**. The pure water flux though the MMM was also studied at different temperatures.

The **Figure 31** compare the flux of pure water and 3D3M solution water flux through MMM. The flux for pure water at 40°C is 17.48 (mol/hr/cm^2*10^5) and goes up to 28.39 (mol/hr/cm^2*10^5) at 50 °C and 41.53 (mol/hr/cm^2*10^5) at 60 °C. The pervaporation mechanism works on solution-diffusion mechanism. The change in temperature generated variation in driving force across the membrane that resulted in increased flux across the membrane. As for 3D3M solution water flux is 17.84 (mol/hr/cm^2*10^5) at 40 °C, 28.93 (mol/hr/cm^2*10^5) at 50 °C and 41.53 (mol/hr/cm^2*10^5) at 60 °C. As it is evident that flux in both cases is similar at corresponding temperatures.

The membrane used for pure Teflon AF2400 pervaporation experiments had thickness of 9.7 µm and the membrane in case of ZIF-8 7.5% had the thickness of 12.1µm. The fluxes for pure Teflon AF2400 normalized for a thickness of 12.1 µm.
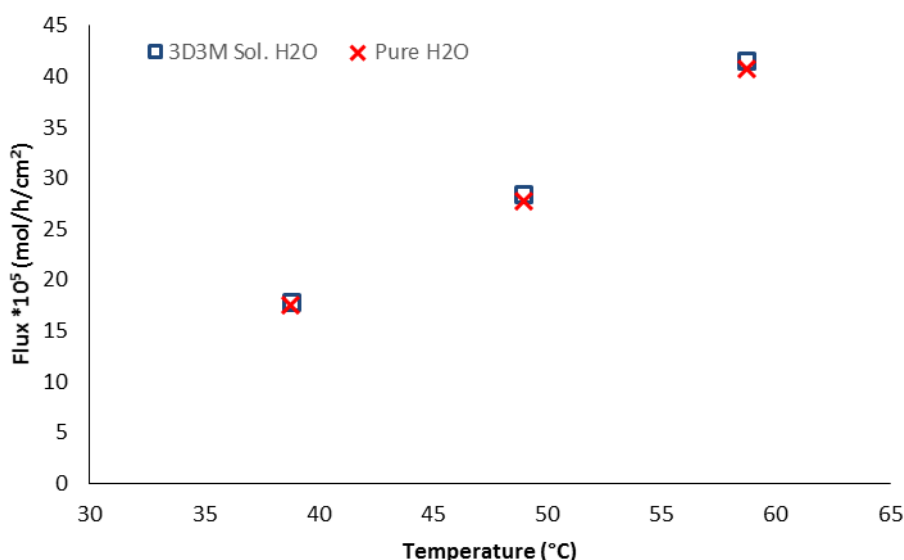
Figure 31: Pure water flux and 3D3M solution water flux as a function of temperature in MMM (membrane thickness 12.1±1.5µm)

Figure 32 shows flux of H_2O for 3D3M solution in pure Teflon AF2400 and ZIF-8 7.5% MMM plotted against temperature. **Figure 32** illustrates that the temperature has a positive effect on

H₂O flux, the thermal energy transformed into mobility of the molecular chains. The flux through the membrane could be analyzed in terms of Arrhenius equation. The activation energies calculated for pure Teflon for H_2O is 0.635 kJ/mol, which shows that increase in temperature has positive impact on the flux. The flux of water in pure Teflon AF2400 is 11.6 (mol/hr/cm^2*10^5) at 40 °C, 19.2 (mol/hr/cm^2*10^5) at 50 °C and 33 (mol/hr/cm^2*10^5) at 60 °C.

As analysis shows that in ZIF-8 7.5% MMM, the flux at every temperature is higher than pure Teflon AF2400. In ZIF-8 the flux at 40 °C corresponds to 17.5 (mol/hr/cm^2*10^5) and 27.8 (mol/hr/cm^2*10^5) at 50 °C and 40.7 (mol/hr/cm^2*10^5) at 60 °C. The possible reason for this trend could be same as observed in permeability results that ZIF-8 disrupted the chain packing and created addition free volume for H₂O molecules to permeate. The calculated activation energy for H_2O in ZIF-8 7.5% is 0.540 kJ/mol. The activation energies depend upon chemical potential and concentration which changes with temperature. The Arrhenius plot for ZIF-8 7.5% MMM is shown in **Figure 53**.
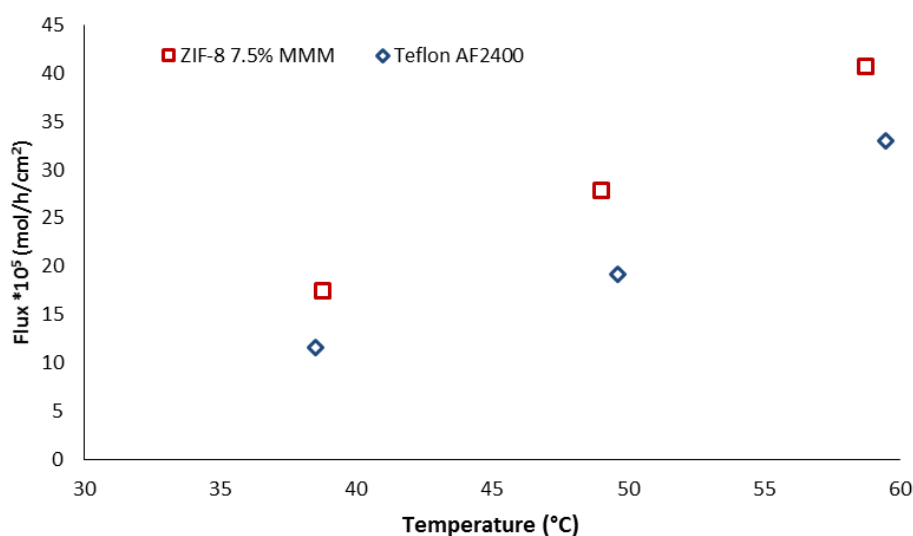
Figure 32: H₂O flux in Teflon AF2400 and AF2400/ZIF-8 for 3D3M solution as a function of operating temperature (membrane thickness 12.1±1.5.µm)

The **Figure 33** and **Figure 34** illustrates the DEEA and MAPA fluxes for 3D3M solution in pure Teflon AF2400 and ZIF-8 7.5% MMM respectively. The effect of temperature is positive for DEEA flux in pure Teflon AF2400 and ZIF-8 7.5% MMM. The activation energies calculated for DEEA are 801 kJ/mol and 747 kJ/mol for pure and mixed matrix respectively.

The flux of DEEA corresponds to 0.051 (mol/hr/cm^2*10^5) at 40 °C, to 0.074 (mol/hr/cm^2*10^5) at 50 °C and 0.195 (mol/hr/cm^2*10^5) at 60 °C in pure Teflon AF 24000. The step increase in the flux at 60 °C is relatively higher. For ZIF-8 7.5% MMM, the inclusion of ZIF-8 particles reduce the flux to 0.027 (mol/hr/cm^2*10^5) at 40 °C, 0.053 (mol/hr/cm^2*10^5) at 50 °C and 0.090 (mol/hr/cm^2*10^5) at 60 °C. The decrease is flux is much higher at 40 °C for DEEA as it drops by 46% and then at 50 °C the reduction in flux becomes 28% and again at 60 °C flux drop is 54%. It suggests that the inclusion of nanoparticles increase the diffusive pathways for DEEA and possibly constricted the free movement of molecular chains at high temperatures. This similar behavior was reported by vane et al. [65] for ethanol-water pervaporation in zeolite/PDMS MMM.
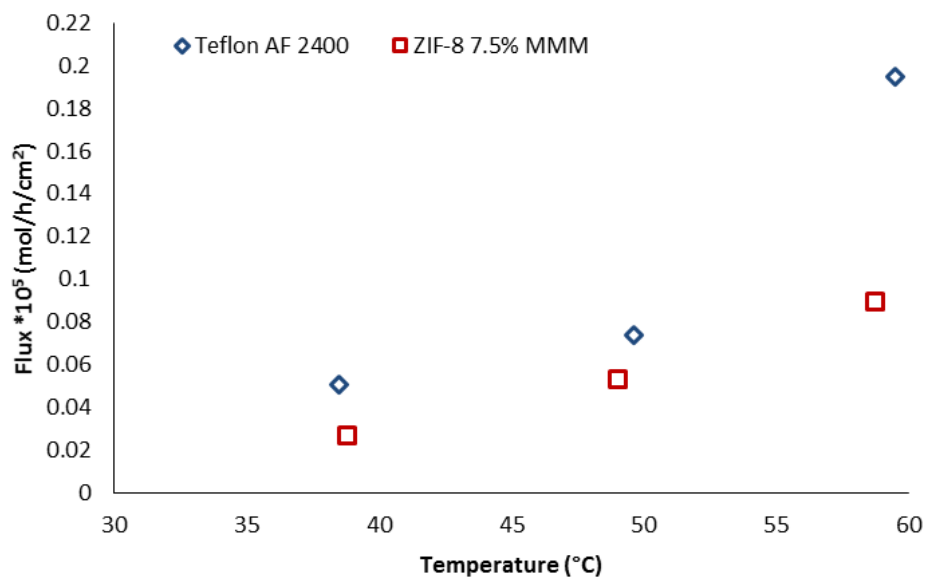
Figure 33: DEEA flux in Teflon AF2400 and AF2400/ZIF-8 for 3D3M solution as a function of operating temperature (membrane thickness 12.1±1.5µm)

The experimental values for MAPA flux obtained in the temperature range of 40-60 °C. The values obtained for pure Teflon AF2400 are 0.043, 0.072 and 0.188 (mol/hr/cm^2*10^5) at the corresponding temperatures of 40, 50 and 60 °C respectively. The activation energy found from Arrhenius equation is 883 kJ/mol.

The flux for ZIF-8 7.5% MMM shows the following trend, 0.0306<0.0617<0.1118 (mol/hr/cm^2*10^5) at 40<50<60 °C. The experimental values calculated from pervaporation setup for ZIF-8 7.5% MMM is lower than pure Teflon AF2400. The activation energy calculated for MAPA in ZIF-8 7.5% MMM is 811 kJ/mol. In contrast with pure Teflon

AF2400, the flux decreased in ZIF-8 7.5% MMM with positive temperature shift for both MAPA and DEEA.

The kinetic size of H_2O is smaller than kinetic sizes of MAPA and DEEA. It can explain the higher flux of water in comparison with MAPA and DEEA.
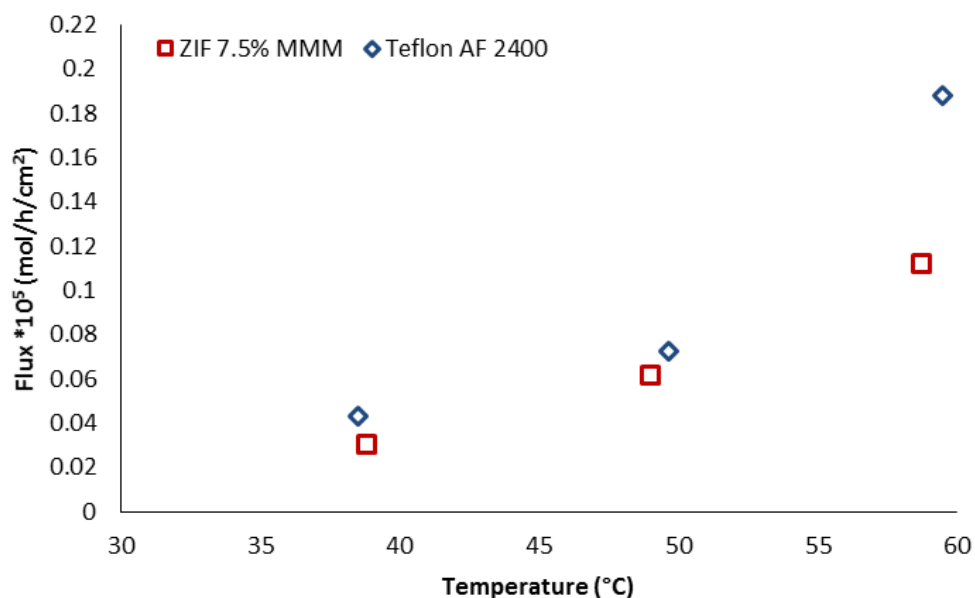
Figure 34: MAPA flux in Teflon AF2400 and AF2400/ZIF-8 for 3D3M solution as a function of operating temperature (membrane thickness 12.1±1.5 µm)

Figure 35 illustrates the ideal selectivity of CO_2 flux versus amine (MAPA+DEEA) flux. As shown in the figure, the MMMs are more selective towards CO_2 in comparison with amines at every experimental temperature. The CO_2/amine selectivity in pure Teflon AF is 394 at 40 °C, decrease to 242 at 50 °C and further decrease to 88 at 60 °C. As for ZIF-8 MMM, the CO_2/amine selectivity is 763 at 40 °C, 378 at 50 °C and 212 at 60 °C. The CO_2/amine ideal selectivity is 2.4 times more than what obtained for pure AF2400 at 60 °C. With an increase in temperature from 40 °C to 60 °C, the MMM CO_2/amine selectivity increase from 1.93 to 2.4.

The possible explanation of this behavior could be that ZIF-8 particles restricted the mobility of molecular chains at higher temperatures. Another possible explanation can be the nanoparticles increase the diffusive pathways for amines. Even though these results are promising but these are ideal selectivity results, as the CO_2 and 3D3M are not permeating simultaneously. These results must be verified using a membrane contactor. The permeability

of CO_2 calculated at 50 °C according to the Arrhenius parameters (activation energy and pre-exponential factor) obtained from the analysis of pure CO_2 permeability data.
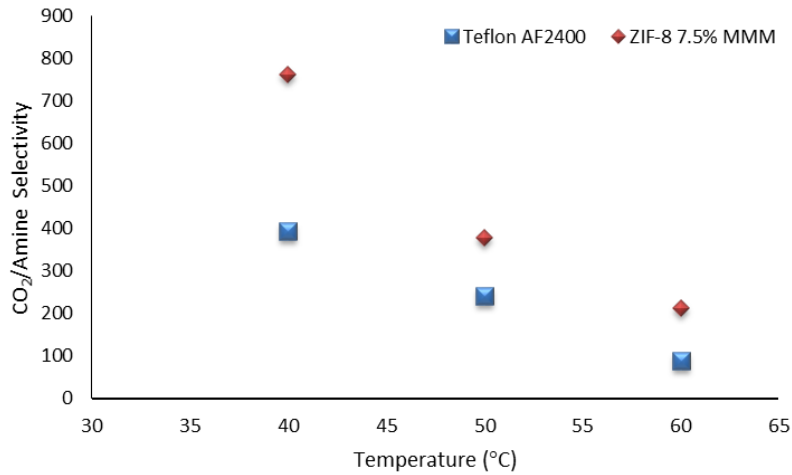
Figure 35: CO_2/Amine Selectivity for at different temperatures

4.3.2 Absorbents with reduced water amount

Another possible solution to reduce the regeneration energy requirement is related to the use of solvent with reduced water content. Therefore, the amine flux through pure Teflon AF2400 was investigated for different MEA concentration of the feed solution. Chabanon et al. [22] studied process intensification to reduce the regeneration energy requirements and increase absorption capacity by increasing amine concentration and the temperature. It was reported that at 60 °C and with 70% MEA concentration the energy requirements were considerably reduced.
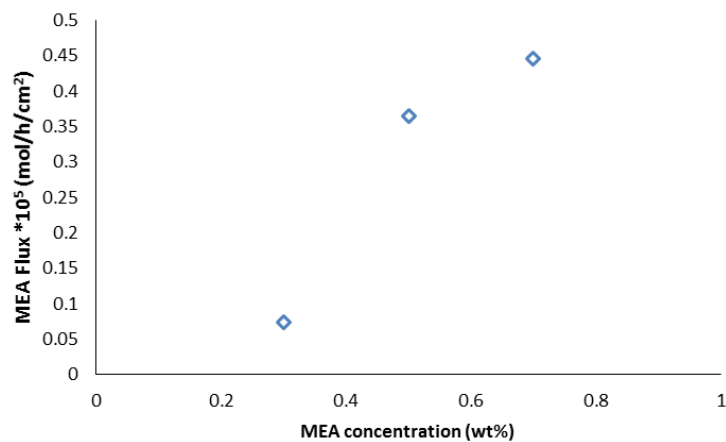
Figure 36: MEA flux as a function of Concentration at 60 °C in pure Teflon AF2400

Figure 36 illustrates the flux of MEA of different concentration at 60 °C, at 30% concentration MEA flux is 0.0735 (mol/hr/cm^2*10^5), at 50% flux is 0.36 (mol/hr/cm^2*10^5) and at 70% corresponding flux is 0.45 (mol/hr/cm^2*10^5). The calculated 3D3M amine flux in pure Teflon AF2400 is 0.38 (mol/hr/cm^2*10^5), which is higher than 50% MEA but lower than 70% MEA solution. The ZIF-8 7.5% MMM are more selective gives lower 3D3M amine flux for all cases except for 30% MEA solution. In addition, the flux of water seems to follow opposite trend; the results are shown in **Figure 37**. The water flux at 30% MEA concentration is 47 (mol/hr/cm^2*10^5), declined to 42 (mol/hr/cm^2*10^5) at 50% and to 30 (mol/hr/cm^2*10^5) at 70%.
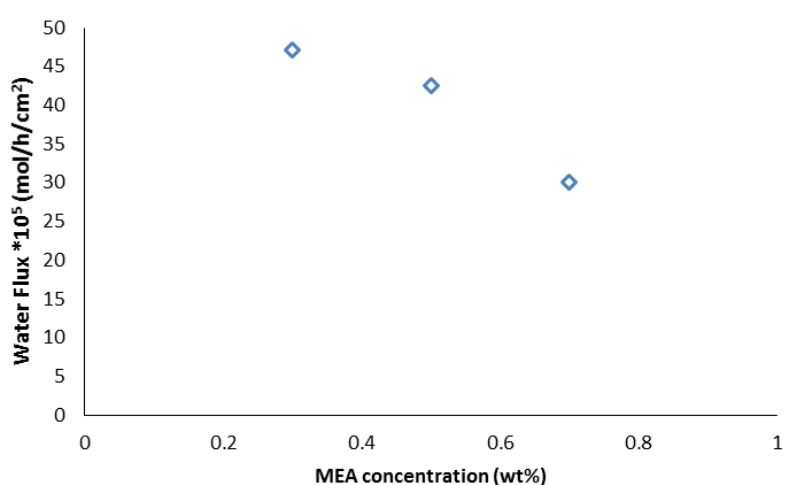
Figure 37: H$_2$O flux as a function of Concentration at 60 °C in pure Teflon AF2400

The CO$_2$/MEA amine ideal selectivity is 460 at 30% concentration, showing promising results. However, the increase in MEA concentration has detrimental effect on selectivity as it drops to 92 at 50% concentration and further to 75 at 70% concentration. The increase in MEA concentration increased its activity coefficient and, thus, the chemical potential across the membrane. As a consequence a larger flux is obtained. The results are shown in **Figure 38**.
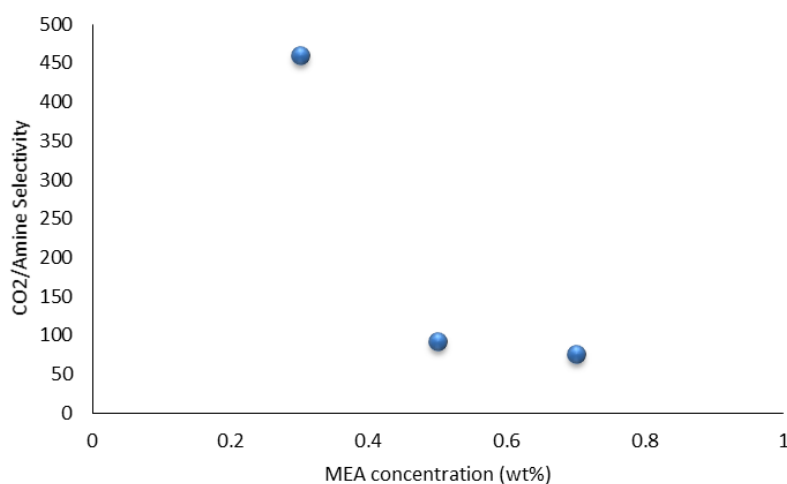
Figure 38: CO2/ MEA amine Selectivity for at different temperatures

4.4 **Vapors Sorption**

Vapor sorption experiments were carried to improve the basic understating of transport mechanisms of MAPA, DEEA and water through Teflon AF2400, which is important for development and optimization of membrane. To the best of author's knowledge, only one paper has been published so far that explains sorption and diffusion of different organic and polar vapors in Teflon AF 2400 polymer [66], but amines were not included. Tokarev et al. [66] studied the sorption and diffusion of different small organic molecules like acetone, ethanol in Teflon AF 2400 membrane at 25 °C. The sorption isotherms of different gases have also been reported in the literature for Teflon AF2400 membranes and they are typically concave to pressure axis and in accordance with dual-mode sorption model [67].

Firstly, sorption experiments were carried out with Teflon AF2400 membrane and Acetone as penetrant to validate the system, since the pressure decay rig was designed and built by Dr. Luca Ansaloni purposely for this study. The Teflon AF 2400 membrane was placed inside the cell and acetone was used as penetrant to ratify with reported data [66]. The acetone also showed the Fickian behavior and comparative analysis of experimental isotherm with literature data result is illustrated in **Figure 39**. The vapor pressure of acetone is 462.22 mbar at 35 °C but due to full scale limitation of pressure transducer, only vapor activity up to 0.2 (100 mbar) was possible.

46
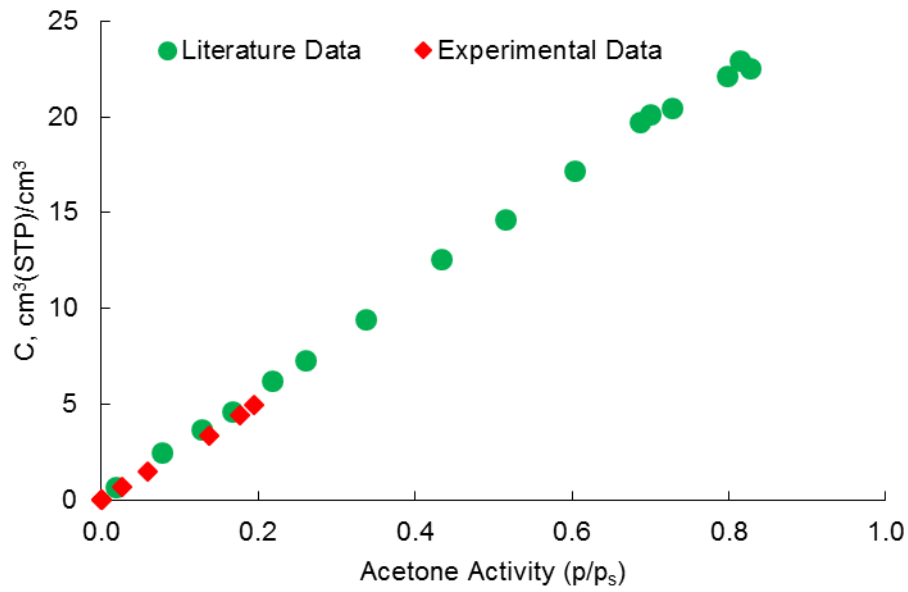
Figure 39: Sorption isotherm of Acetone at 25°C in Teflon AF2400

The sorption isotherm for acetone is linear and in good agreement with literature data [66]. The Fickian curve (at vapor activity of 0.13) and kinetics of sorption of acetone at various vapor activities are displayed in **Figure 40** and **Figure 41** respectively. The solute showed a proper Fickian behavior for all the steps performed.
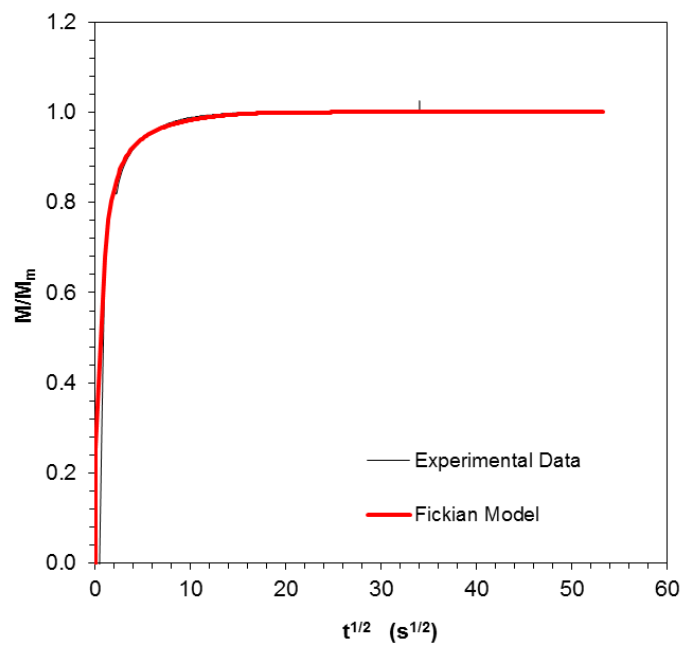
Figure 40: Fickian curve and experimental point for acetone
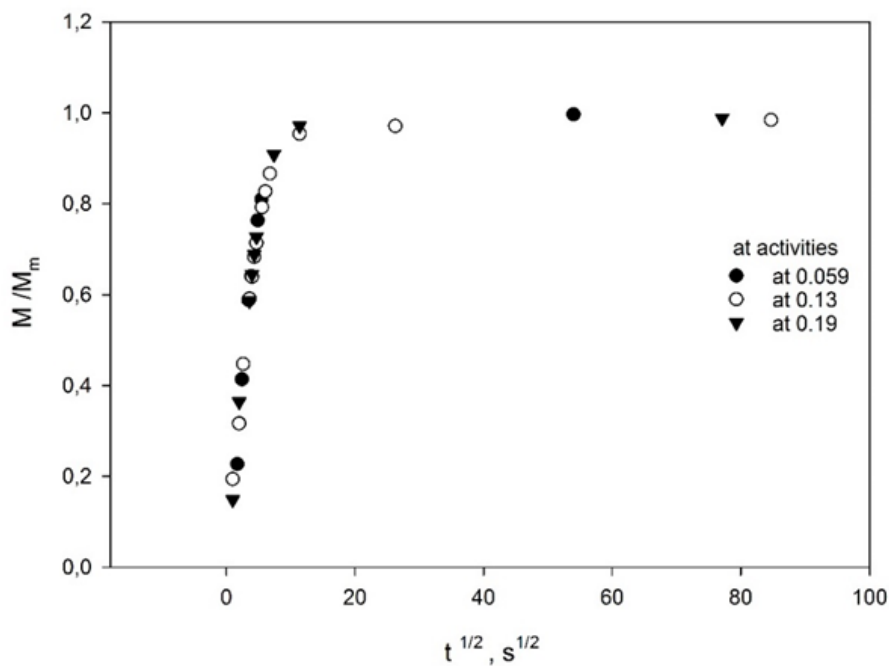
Figure 41: Kinetics of sorption for acetone at 25 °C in Teflon AF2400.

The isotherm of DEEA, MAPA and H_2O reveal linear behaviors, as shown in **Figure 42**, **Figure 43** and **Figure 44** respectively. The DEEA sorption isotherm studied at different vapor activities and solubility increases linearly increase in vapor activity. The vapor and Fickian model for DEEA shown in **Figure 47**.
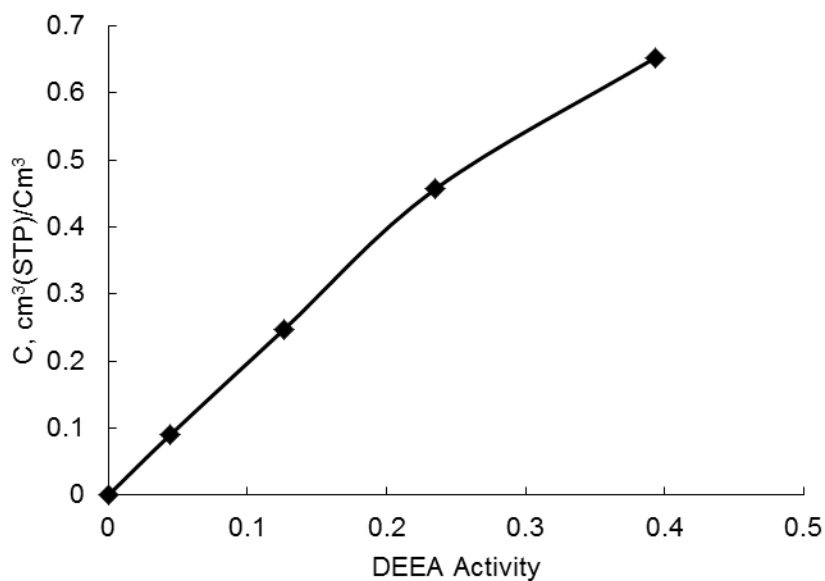
Figure 42: Sorption isotherm of DEEA at 35 °C

The isotherm of MAPA is linear as shown in **Figure 43**. A single data point shown in **Figure 43** took two or more days to reach a steady state value. The solubility of MAPA was 0.55 cc (STP)/cc at the vapor activity of 0.10. At the vapor activity of 0.25, the solubility goes up to 1.23 cc (STP)/cc. The calculated solubility at vapor activity of 0.5 is 2.97 cc (STP)/cc. The kinetic of sorption and Fickian model (at vapor activity of 0.26) for MAPA illustrated in **Figure 45**.
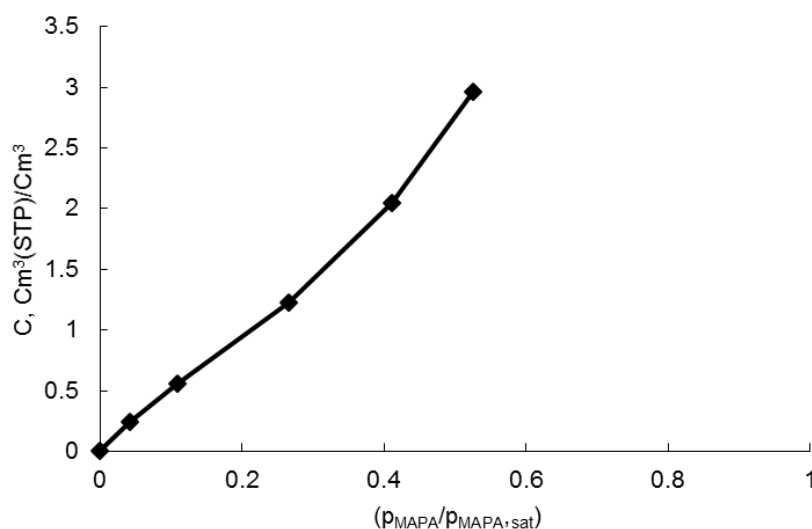
Figure 43: Sorption isotherm of MAPA at 35 °C

The polar compounds in hydrophobic polymers reported to form clusters and isotherm concave to the concentration axis [68], [69]. The isotherm for water shown in **Figure 44**. It can be postulated that no cluster formation and sorption isotherm is linear, likely due to the hydrophobic nature of the materials, coupled with the large free volume. The approximated solubility at vapor activity of 0.17 is 0.84 cm^3 (STP)/cm^3. At vapor activity of 0.53 corresponding solubility is 1.58 cm^3(STP)/cm^3. The solubility of H_2O (at activity of 0.5) appears lower than MAPA solubility. It can be suggested, the highly hydrophobic nature of polymer is responsible for this behavior. The experiments were repeated twice to validate the isotherm behaviors.
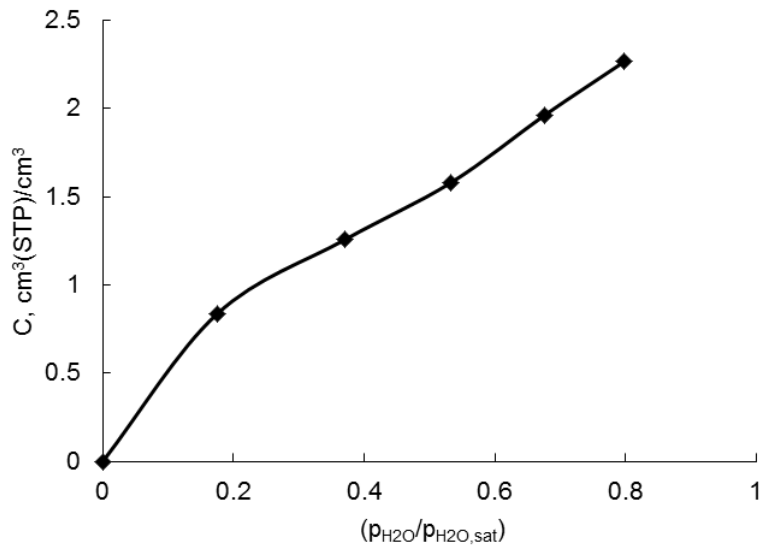
Figure 44: Sorption isotherm of water at 35 °C

The solute concentrations in Teflon AF2400, at the vapor activity of 0.4, of all three penetrant are 0.00436, 0.00430 and 0.00076 g/g for MAPA, DEEA and water respectively. For water, even at the vapor activity close to one, solubility remains 0.0010 g/g_{pol}.

The analysis of every single step of the sorption isotherm allows understanding the diffusion dependence of MAPA, H_2O and DEEA with concentration in the membrane matrix. However, all the three components showed a non-Fickian evolution, most likely related to possible clustering that is taking place in the matrix during the time evolution of the single step. This type of phenomena are likely to happen for polar components and the large free volume nature of the matrix can allow faster interactions between the penetrant molecules, more than with the polymer chains, giving raise to the non-Fickian behavior reported in the **Figure 45**, **Figure 46** and **Figure 47**.

The diffusion coefficients estimated by best fitting of Fickian curve. The diffusion coefficient of MAPA is order of magnitude 10^9 cm^2/s and for DEEA 10^{10} cm^2/s. It can be speculated that branched structure of DEEA is responsible for the behavior.
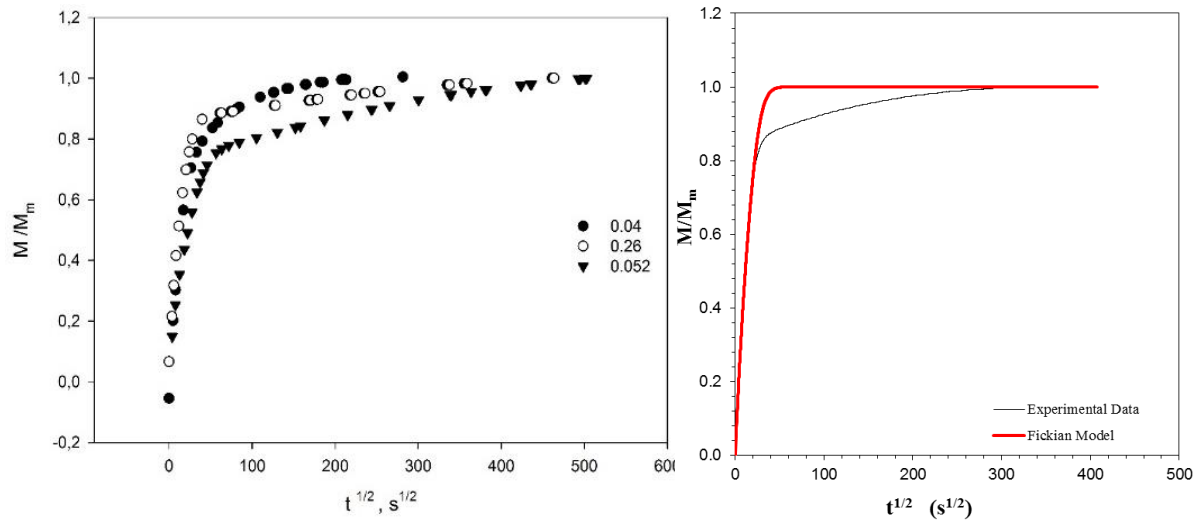
Figure 45: Kinetic of sorption and Fickian model in MAPA
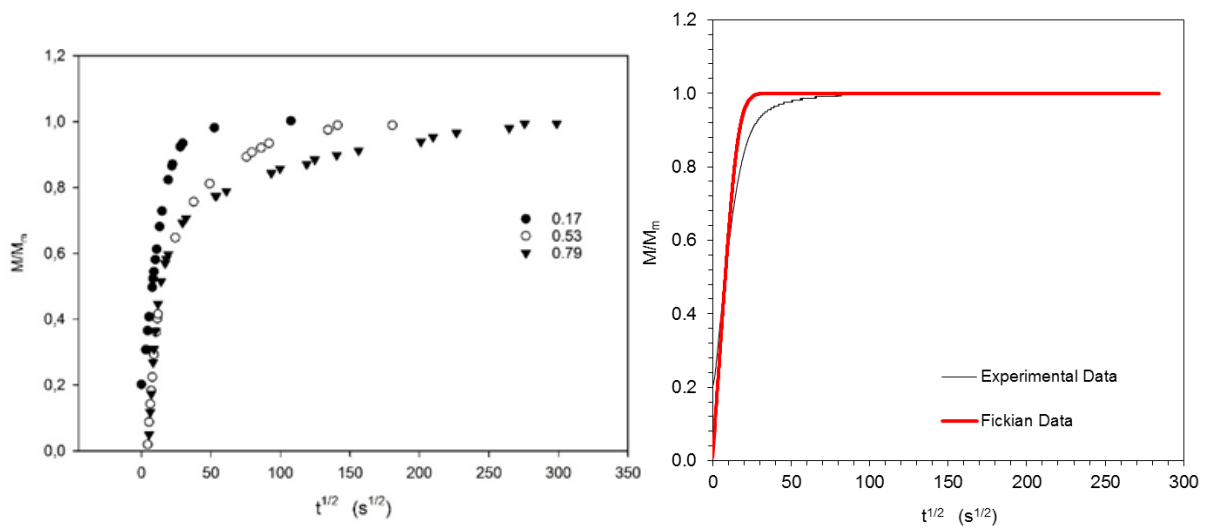
Figure 46: Kinetic of sorption and Fickian model in H_2O
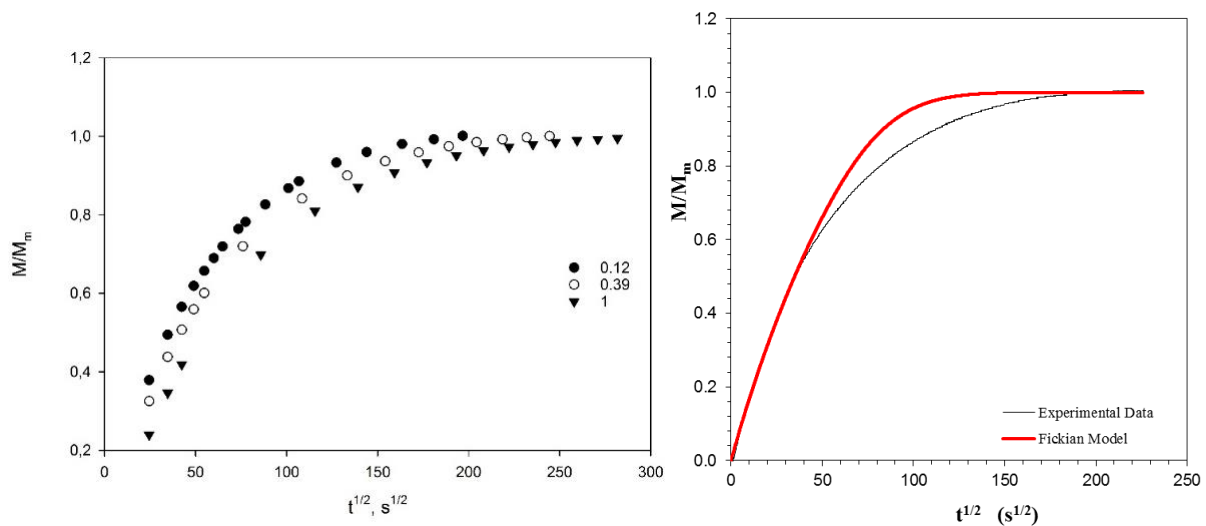
Figure 47: Kinetic of sorption and Fickian model DEEA

5 Conclusion

The aim of the present project was to develop a dense layer with superior CO_2/amine selectivity compared to the one obtained by using pure Teflon AF2400, that can be used for the preparation of thin composite membranes to be used in membrane contactors. For this reason, different mixed matrix membranes were studied to achieve superior amine barrier properties.

In the first part, the gas permeation experiments were performed for pure Teflon AF2400 and with different fillers (RGO and ZIF-8) and loadings (2-10 wt%) to have a comparative analysis. The results suggested that MMMs possess a larger CO_2 permeability at every experimental temperature compared to pure Teflon AF2400. For 10 wt% ZIF-8/Teflon AF2400 MMM, the increase in CO_2 permeability was 35% and in case of 10 wt% RGO/Teflon AF2400 MMM increase was 23%. However, the ZIF-8/Teflon AF 2400 at loading 10 wt% MMM showed visible particles aggregation on the membrane surface. The 10 wt% RGO/Teflon AF 2400 MMM showed an increase of the stiffness of the membrane layer, which became much more brittle. The permeation results for RGO and ZIF-8 MMMs at different loading suggested that ZIF-8/Teflon AF2400 with 7.5 wt% loading gives better results.

The morphological of MMMs was investigated by scanning electron microscope. The SEM results showed that 10% RGO and 7.5 wt% ZIF-8 MMM have a good dispersion of inorganic phase with no visible voids. As for 10 wt% ZIF-8 MMM, the sieve in cage morphology was obtained.

For the first time the amine transport through pure Teflon AF2400 and 7.5 wt% ZIF-8 MMM layer was studied. MMM have lower fluxes for MAPA and DEEA in comparison with Teflon AF2400 at every experimental temperature. For 7.5 wt% ZIF-8 MMM, the ideal CO_2/3D3M amine selectivity is 763 at 40 °C, 378 at 50 °C and 212 at 60 °C. The ideal CO_2/amine selectivity for 7.5 wt% ZIF-8 MMM is 1.93 times higher than pure Teflon AF2400 at 40°C and 2.4 times higher at 60 °C.

Finally, the sorption experiments were carried out in the pressure decay rig to develop a better understanding of transport mechanism, especially for amines, as no literature data is available. The solubility for MAPA and DEEA was found to be around 0.00436, 0.00430 g/g_{pol}. The low solubility of amines implied the low permeation rate for amines, as visible in pervaporation experiments. For water, even at the activity close to one, the solubility was 0.001 g/g_{pol}.

6 **Future Research**

As the selectivity results showed that MMM are more CO_2 selective than pure Teflon AF2400. The next step would be finding a process for the successful coating of thin mixed matrix membrane on porous module and test it in membrane contactor.

Another approach could be to further, characterize membrane with DSC to look for change in glass transition temperature and study the transport behavior of the proposed MMM under humidified gas conditions over the whole RH range. Indeed, the CO_2 permeability is expected to decrease at increasing the RH, but the extent could be limited in view of the hydrophobicity of the membrane layer. In addition, test MMM with different loading of ZIF-8 and RGO in pervaporation setup can be carried out to estimate how the nanoparticles loading affect the amine flux through the membrane.

About the fundamental characterization carried out with the sorption setup, it will be interesting to investigate deeper the non-Fickian behavior showed by the amines, trying to find a theoretical description able to describe the real diffusion coefficient. In addition, test with MMMs should be carried out in order to find how the nanoparticles embedded within the matrix affect the solubility and the diffusion of the amines.

Bibliography

[1] S. Zhao, P. H. Feron, . L. Deng, E. Favre, E. Chabanon, S. Yan, J. Hou, V. Chen and H. Qi, "Status and progress of membrane contactors in post-combustion carbon capture: A state-of-the-art review of new developments," *Journal of Membrane Science,* vol. 511, pp. 180-206, 2016.

[2] L. Carter, "Retrofitting Carbon Capture Systems on Existing Coal-fired Power Plants," American Public Power Association, Washington, D.C., 2007.

[3] R. R. B. (. Corp.), "Separating acid gases". Patent U.S. Patent 1783901, 1930.

[4] A. Tobiesen, E. F. d. Silva, H. M. Kvamsdal, K. Hoff, H. Knuutila and T. Mejdell, "Evaluation-novel-post-combustion-co2-capture-solvent-concepts," IEA Greenhouse Gas R&D Programme (IEAGHG), 2009.

[5] A. Gabelman and S.-T. Hwang, "Hollow fiber membrane contactors," *Journal of Membrane Science,* vol. 159, pp. 61-106, 1999.

[6] M. Mavroudi, S. Kaldis and G. Sakellaropoulos, "Reduction of CO2 emissions by a membrane contacting process," *FUEL,* vol. 82, pp. 2153-2159, 2003.

[7] A. Gabelman and S.-T. Hwang, "Hollow Fiber membrane contactors," *Journal of Membrane Science,* vol. 159, pp. 61-106, 1999.

[8] Naional energ technology Lab. , "Pre-Combustion Carbon Capture by a Nanoporous, Superhydrophobic Membrane Contactor Process," June 2011. [Online]. Available: www.netl.doe.gov. [Accessed 20 June 2016].

[9] C. Scholes, A. Qader, G. Stevens and S. Kentish, "Membrane Gas-Solvent Contactor Pilot Plant Trials of CO2 Absorption from Flue Gas," vol. 49, no. 16, 2014.

[10] A. Arif, "Carbon Dioxide Capture Using Membrane Contactor- Membrane Material Development," Norwegian University of Science and Technology , Trondheim , 2016.

[11] L. Ansaloni,, R. Rennemo, H. Knuutila and l. Deng, "3rd Generation Membrane Contactors: amine permeation through the membrane interface," UT-CCS, Austin, Texas, February 2016.

[12] E. Chabanon, D. Roizard and . E. Favre, "Membrane Contactors for Postcombustion Carbon Dioxide Capture: A Comparative Study of Wetting Resistance on Long Time Scales," *Industrial & Engineering Chemistry Reserach.*

[13] M. W. Arshad, . H. F. Svendsen, P. L. Fosbøl, N. v. Solms and K. Thomsen, "Equilibrium Total Pressure and CO2 Solubility in Binary and Ternary Aqueous Solutions of 2-(Diethylamino)ethanol (DEEA) and 3-(Methylamino)propylamine (MAPA)," 2014.

[14] A. F. Ciftja, A. Hartono and S. F. Hallvard, "Experimental study on phase change solvents in CO2 capture by NMR spectroscopy," *Chemical Engineering Science,* vol. 102, pp. 378-386, 2013.

[15] D. . D. Pinto, S. A. Zaidy, A. Hartono and H. F. Svendsen, "Evaluation of a phase change solvent for CO2 capture: Absorption and desorption tests," *International Journal of Greenhouse Gas Control,* vol. 28, pp. 318-327, 2014.

[16] R. P. Mayer and R. A. Stowe , "MERCURY POROSIMETRY--BREAKTHROUGH PRESSURE FOR PENETRATION BETWEEN PACKED SPHERES," *JOURNAL OF COLLOID SCIENCE,* vol. 20, pp. 893-911, 1965.

[17] J. A. Franco, . S. E. Kentish, J. M. Perera and G. W. Stevens, "Poly(tetrafluoroethylene) Sputtered Polypropylene Membranes for Carbon Dioxide Separation in Membrane Gas Absorption," vol. 50, no. 7, 2011.

[18] F. Bougie and . M. C. Iliuta, "Analysis of Laplace–Young equation parameters and their influence on efficient CO2 capture in membrane contactors," *Separation and Purification Technology,* vol. 118, pp. 806-815, 2013.

[19] R. Wang, D. Li, C. Zhou, M. Liu and D. Liang, "Impact of DEA solutions with and without CO2 loading on porous polypropylene membranes intended for use as contactors," *Journal of Membrane Science,* vol. 229, no. 1-2, pp. 147-157, 2004.

[20] "Wetting of polypropylene hollow fiber membrane contactors," *Journal of Membrane Science,* vol. 362, no. 1-2, pp. 444-452, 2010.

[21] M. Mavroudi, S.P. Kaldis and G.P. Sakellaropoulos, "Reduction of CO2 emissions by a membrane contacting process," vol. 82, no. 15-17, 2003.

[22] E. Chabanon, R. Bounaceur, C. Castel, S. Rode, D. Roizard and . E. Favre, "Pushing the limits of intensified CO2 post-combustion capture by gas–liquid absorption through a membrane contactor," vol. 91, May 2015.

[23] . S. Stern, V. Shah and B. Hardy, "Structure-permeability relationships in silicone polymers," vol. 25, no. 6, 1987.

[24] H. Al-saffar, B. Ozturk and R. Hughes, "A Comparison of Porous and Non-Porous Gas-Liquid Membrane Contactors for Gas Separation," *Chemcial Engineering Research and Design,* vol. 75, no. 7, pp. 685-692, 1997.

[25] P. Nguyen, E. Lasseuguette, . Y. Medina-Gonzalez, J. Remigy, D. Roizard and . E. Favre, "A dense membrane contactor for intensified CO2 gas/liquid absorption in post-combustion capture," *Journal of Membrane Science,* vol. 377, no. 1-2, pp. 261-272, 2011.

[26] H. A. Rangwala, "Absorption of carbon dioxide into aqueous solutions using hollow fiber membrane contactors," vol. 112, no. 2, 1996.

[27] R. W. Baker, MEMBRANE TECHNOLOGY AND APPLICATIONS- 2nd Edition, John Wiely & Sons, Ltd, March 2004.

[28] H. B. T. Jeazet, C. Staudt and C. Janiak, "Metal–organic frameworks in mixed-matrix membranes for gas separation," *Royal society of chemistry,* vol. 41, pp. 14003-14027, 2012.

[29] M. Mulder, Basic Principles of Membrane Technology, Kluwer Academic Publisher, 1996.

[30] W. J. Koros and G. K. Fleming, "Membrane-based gas separation," *Journal of Membrane Science,* vol. 83, p. 80, 1993.

[31] I. Pinnau and . L. G. Toy , "Gas and vapor transport properties of amorphous perfluorinated copolymer membranes based on 2,2-bistrifluoromethyl-4,5- difluoro-1,3-dioxole/tetrafluoroethylene," *Journal of Membrane Science* , vol. 109, pp. 125-133, 1996.

[32] T.-S. Chung, L. Y. Jiang, Y. Li and S. Kulprathipanja, "Mixed matrix membranes (MMMs) comprising organic polymers with dispersed inorganic fillers for gas separation," *Progress in Polymer Science,* vol. 32, no. 4, pp. 483-507, 2007.

[33] L. M. Robeson , "Correlation of separation factor versus permeability for polymeric membranes," *Journal of Membrane Science, ,* vol. 62, pp. 165-182, 1991.

[34] M. C. Ferrari, M. Galizia, M. G. D. Angelis and . C. S. Giulio, "Gas and Vapor Transport in Mixed Matrix Membranes Based on Amorphous Teflon AF1600 and AF2400 and Fumed Silica," vol. 49, no. 23, 2010.

[35] M. Aroon, A. Ismail, T. Matsuura and . M. Montazer-Rahmati, "Performance studies of mixed matrix membranes for gas separation: A review," *Separation and Purification Technology,* vol. 75, no. 3, pp. 229-242, 2010.

[36] R. Barrer and S. James, "ELECTROCHEMISTRY OF CRYSTAL—POLYMER MEMBRANES. PART I. RESISTANCE MEASUREMENTS," *The Journal of Physical chemistry ,* vol. 64, no. 4, pp. 417-421, 1960.

[37] J. Duval, *Adsorbent filled polymeric membranes. PhD thesis,* The Netherlands: University of Twente;, 1995.

[38] *Transport through zeolite filled polymeric,Ph. D. Thesis,* The Netherlands: University of Twente, 1994.

[39] Y. Li, T.-S. Chung, C. Cao and S. Kulprathipanja, "The effects of polymer chain rigidification, zeolite pore size and pore blockage on polyethersulfone (PES)-zeolite A mixed matrix membranes," *Journal of Membrane Science,* vol. 260, no. 1-2, pp. 45-55, 2005.

[40] M. Moaddeb and W. J. Koros, "Gas transport properties of thin polymeric membranes in the presence of silicon dioxide particles," *Journal of Membrane Science,* vol. 125, no. 1, pp. 143-163, 1997.

[41] G. Clarizia, . C. Algieri and . E. Drioli, "Filler-polymer combination: a route to modify gas transport properties of a polymeric membrane," *Polymer,* vol. 45, no. 16, pp. 5671-5681, 2004.

[42] A. F. Ismail , . K. . C. Khulbe and . T. Matsuura , Gas Separation Membranes Polymeric and Inorganic, Springer International Publishing Switzerland , 2015.

[43] R. Nasir, H. Mukhtar, Z. Man and D. F. Mohshim, "Material Advancements in Fabrication ofMixed-Matrix Membranes," *Chemical Engineering & Technology,* vol. 36, no. 5, pp. 717-727, 2013.

[44] Z. Luo, Y. Lu, L. A. Somers and A. T. C. Johnson, "High Yield Preparation of Macroscopic Graphene Oxide Membranes," *Journal of the American Chemical Society,* vol. 131, no. 3, pp. 898-899, 2009.

[45] L. Olivieri, S. Ligi, M. G. D. Angelis, G. Cucca and A. Pettinau, "Effect of Graphene and Graphene Oxide Nanoplatelets on the Gas Permselectivity and Aging Behavior of PTMSP," vol. 54, 2015.

[46] H. Bux, . F. Liang, Y. Li, . J. Cravillon, . M. Wiebcke and . J. Caro, "Zeolitic Imidazolate Framework Membrane with Molecular Sieving Properties by Microwave-Assisted Solvothermal Synthesis," *J. Am. Chem. Soc.,* vol. 131, no. 44, pp. 16000-16001, 2009.

[47] K. S. Park, Z. Ni, A. P. Coˆteˊ, J. Y. Choi, . R. Huang, F. J. Uribe-Romo, H. K. Chae, M. O'Keeffe and . O. M. Yaghi, "Exceptional chemical and thermal stability of zeolitic imidazolate frameworks," *Proceeding of the National Academy of Science ,* vol. 103, no. 27, pp. 10186-10191, 2006.

[48] M. J. C. Ordoñez, K. J. Balkus Jr, J. P. Ferraris and I. H. Musselman, "Molecular sieving realized with ZIF-8/Matrimid® mixed-matrix membranes," *Journal of Membrane Science,* vol. 361, no. 1-2, pp. 28-37, 2010.

[49] M. J. C. Ordoñez, . K. . J. Balkus Jr., J. P. Ferraris and I. H. Musselman, "Molecular sieving realized with ZIF-8/Matrimid® mixed-matrix membranes," *Journal of Membrane Science,* vol. 361, no. 1-2, pp. 28-37, 2010.

[50] V. Nafisi and M.-B. Hägg, "Gas separation properties of ZIF-8/6FDA-durene diamine mixed matrix membrane," *Separation and Purification Technology,* vol. 128, pp. 31-38, 2014.

[51] R. S. Murali, S. Sridhar, T. Sankarshana and Y. V. L. Ravikumar, "Gas Permeation Behavior of Pebax-1657 Nanocomposite Membrane Incorporated with Multiwalled Carbon Nanotubes," *Ind. Eng. Chem,* vol. 49, no. 14, pp. 6530-6538, 2010.

[52] J.-M. Duval, . B. Folkers, . M. Mulder, G. Desgrandchamps and C. Smolders, "Adsorbent filled membranes for gas separation. Part 1. Improvement of the gas separation properties of polymeric membranes by incorporation of microporous adsorbents," *Journal of Membrane Science,* vol. 80, no. 1-2, pp. 189-198, 1993.

[53] D. Q. Vu, . W. J. Koros and . S. J. Miller, "Mixed matrix membranes using carbon molecular sieves: I. Preparation and experimental results," *Journal of Membrane Science,* vol. 211, no. 2, pp. 311-334, 2003.

[54] 3M, [Online]. Available: http://multimedia.3m.com/mws/media/64892O/fluorinert-electronic-liquid-fc-72.pdf. [Accessed 16 7 2016].

[55] B. Zornoza, C. Tellez, J. Corona, J. Gascon and F. Kapteijn, "Metal organic framework based mixed matrix membranes: An increasingly important field of research with a large application potential," *Microporous and Mesoporous Materials,* vol. 166, no. 15, pp. 67-78, 2013.

[56] L. Ansaloni, "Polymeric membranes for CO2 Separation: Effect of aging and humidity facilitated transport," Alma Mater Studiorum- University of Bologna , 2014.

[57] J. Crank, The Mathematics of Diffusion, Oxford: Clarendon, 1975.

[58] N. L. Torad, . M. Hu, . Y. Kamachi, K. Takai, M. Imura, M. Naito and Y. Yamauchi, "Facile synthesis of nanoporous carbons with controlled particle sizes by direct

carbonization of monodispersed ZIF-8 crystals," *Royal Society of Chemistry,* vol. 49, pp. 2512-2523, 2013.

[59] T. C. Merkel, I. Pinnau, R. Prabhakar and B. D. Freeman, "Gas and vapor transport properties of perfluorpolymers," in *Materials Science of Membranes for Gas and Vapor Separation*, 2006, pp. Chapter 9, 251-270.

[60] j. C. Jansen, K. Friess and E. Drioli, "Organic vapour transport in glassy perfluoropolymer membranes: A simple semi-quantitative approach to analyze clustering phenomena by time lag measurements," *Journal of Membrane Science,* vol. 367, no. 1-2, pp. 141-151, 2011.

[61] T. Masuda, . Y. Iguchi, B.-Z. Tang and . T. Higashimura , "Diffusion and solution of gases in substituted polyacetylene membranes," *Polymer,* vol. 29, no. 11, pp. 2041-2049, 1988.

[62] T. C. Merkel, B. D. Freeman, R. J. Spontak, Z. He, I. Pinnau, P. Meakin and A. Hill, "Sorption, Transport, and Structural Evidence for Enhanced Free Volume in Poly(4-methyl-2-pentyne)/Fumed Silica Nanocomposite Membranes," *Chemistry of Materials,* vol. 15, no. 1, pp. 109-123, 2003.

[63] J. Ahn, W.-J. Chung, . I. Pinnau and M. D. Guiver, "Polysulfone/silica nanoparticle mixed-matrix membranes for gas separation," *Journal of Membrane Science,* vol. 314, no. 1-2, pp. 123-133, 2008.

[64] J. G. S. Monteiro, H. Majeed, . H. Knuutila and H. F. Svendsen, "Kinetics of CO2 absorption in aqueous blends of N,N-diethylethanolamine (DEEA) and N-methyl-1,3-propane-diamine (MAPA)," *Chemical Engineering Science,* vol. 129, pp. 145-155, 2016.

[65] L. M. Vane, . V. V. Namboodiri and T. C. Bowen, "Hydrophobic zeolite–silicone rubber mixed matrix membranes for ethanol–water separation: Effect of zeolite and silicone component selection on pervaporation performance," *Journal of Membrane Science,* vol. 308, no. 1-2, pp. 230-241, 2008.

[66] A. Tokarev, K. Friess, J. Machkova, M. Šipek and Y. Yampolskii, "Sorption and diffusion of organic vapors in amorphous Teflon AF2400," *Journal of Polymer Science,* vol. 44, no. 5, pp. 832-844, 2006.

[67] T. C. Merkel, V. Bondar, K. Nagai, B. D. Freeman and Y. P. Yampolskii, "Gas Sorption, Diffusion, and Permeation in Poly(2,2-bis(trifluoromethyl)-4,5-difluoro-1,3-dioxole-co-tetrafluoroethylene)," *Macromolecules,* vol. 32, no. 25, pp. 8427-8440, 1999.

[68] P. E. RouseJr., "Diffusion of Vapors in Films," *J. Am. Chem. Soc.,* vol. 69, no. 5, pp. 1068-1073, 1947.

[69] "The sorption and diffusion of water in silicone rubbers: Part I. Unfilled rubbers," *Journal of Macromolecular Science, Part B: Physics,* vol. 3, no. 4, pp. 645-672, 1969.

[70] A. K. Pabby, S. . S. Rizvi and A. M. S. Requena, Handbook of Membrane Separations: Chemical, Pharmaceutical, Food, and Biotechnological Applications, Second Edition ed., CRC PRESS, 2015.

[71] S. Kanehashi and K. Nagai, "Analysis of dual-mode model parameters for gas sorption in glassy polymers," *JOURNAL OF MEMBRANE SCIENCE,* vol. 253, no. 1, pp. 117-138, 2005.

[72] M. Rezakazemi, A. E. Amooghin, M. M. Montazer-Rahmati, A. F. Ismail and T. Matsuura, "State-of-the-art membrane based CO2 separation using mixed matrix membranes (MMMs): An overview on current status and future directions," *Progress in Polymer Science,* vol. 39, no. 5, pp. 817-861, 2014.

[73] R. R. Tiwari, Z. P. Smith, H. Lin, B. Freeman and D. Paul, "Gas permeation in thin films of "high free-volume" glassy perfluoropolymers: Part I. Physical aging," *Polymer,* vol. 55, no. 22, pp. 5788-5800, 2014.

[74] N. Schmeling, R. Konietzny, D. Sieffert, P. Rölling and . C. Staudt, "Functionalized copolyimide membranes for the separation of gaseous and liquid mixtures," *Beilstein Journal of Orgainc Chemistry,* vol. 6, pp. 789-800, 2010.

[75] "Purdue University," Purdue University, West Lafayette, [Online]. Available: https://www.purdue.edu/ehps/rem/rs/sem.htm. [Accessed 27 11 2015].

[76] Ş. Tantekin-Ersolmaz, Ç. Atalay-Oral, . M. Tatlıer, A. Erdem-Şenatalar, B. Schoeman and J. Sterte, "Effect of zeolite particle size on the performance of polymer–zeolite mixed matrix membranes," *Journal of Membrane Science,* vol. 175, no. 2, pp. 285-288, 2000.

[77] R. Mahajan and W. J. Koros, "Factors Controlling Successful Formation of Mixed-Matrix Gas Separation Materials," *Industrial & Engineering Chemistry Reserach,* vol. 39, no. 8, pp. 2692-2696, 2000.

[78] T.-S. Chung, L. Y. Jiang, Y. Li and S. Kulprathipanja, "Mixed matrix membranes (MMMs) comprising organic polymers with dispersed inorganic fillers for gas separation," *Progress in Polymer Science,* vol. 32, no. 4, pp. 483-507, 2007.

[79] T. Masuda, E. Isobe, T. Higashimura and K. Takada, "Poly[1-(trimethylsilyl)-1-propyne]: a new high polymer synthesized with transition-metal catalysts and characterized by extremely high gas permeability," *Journal of the American Chemical Society,* vol. 105, no. 25, pp. 7473-7474, 1983.

[80] . E. C. Suloff , "Sorption Behavior of an Aliphatic Series of Aldehydes in the Presence of Poly(ethylene terephthalate) Blends Containing Aldehyde Scavenging Agents," VTech Works, 2002.

[81] G. Q. Chen, C. A. Scholes, C. M. Doherty, A. J. Hill, G. G. Qiao and S. E. Kentisha, "Modeling of the sorption and transport properties of water vapor in polyimide membranes," *Journal of Membrane Science,* Vols. 409-410, pp. 69-104, 2012.

[82] J. H. Petropoulos, "A comparative study of approaches applied to the permeability of binary composite polymeric materials," *Journal of Polymer Science Part B: Polymer Physics Explore this journal,* vol. 23, no. 7, pp. 1309-1324, 1985.

[83] R. Bouma, A. Checchetti, G. Chidichimo and E. Drioli, "Permeation through a heterogeneous membrane: the effect of the dispersed phase," *Journal of Membrane Science,* vol. 128, no. 2, pp. 141-149, 1997.

[84] T. T. Moore and W. J. Koros, "Non-ideal effects in organic–inorganic materials for gas separation membranes," *Journal of Molecular Structure,* vol. 739, no. 1-3, pp. 87-89, 2005.

[85] W. Koros and R. Chern, Handbook of separation process technology, New York: Ronald W. Rousseau, Ed., John Wiley and Sons, Inc., 1987.

[86] J. C. Lotters, W. Olthuis, P. Veltink and P. Bergveld, "The mechanical properties of the rubber elastic polymer polydimethylsiloxane for sensorapplications," *J. Micromech. Microeng,* vol. 7, pp. 1245-147, 1997.

[87] "CO2CRC Limited," [Online]. Available: http://www.co2crc.com.au/aboutccs/cap_membranes.html. [Accessed 15 04 2016].

[88] Arkhangel'skii, V. Chalykh, A. Rudoi and V. Ogarev, "Diffusion and sorption of hydrocarbons and alcohols in poly(dimethylsiloxane)," *Vysokomolekulyarnye Soedineniya, Seriya B: Kratkie Soobshcheniya,* vol. 19, no. 12, pp. 891-894, 1977.

[89] G. R. Mauze and S. A. Stern, "The dual-mode solution and transport of water in poly(acrylonitrile)," *Polymer Engineering & Science,* vol. 23, no. 10, pp. 548-555, 1983.

[90] T. Borjigin, F. Sun, J. Zhang, K. Cai, H. Ren and G. Zhu, "A microporous metal–organic framework with high stability for GC separation of alcohols from water," *Chem. Commun,* vol. 48, pp. 7613-7615, 2012.

[91] A. Muhammad, M. I. A. Mutalib, C. D. Wilfred, T. Murugesan and A. Shafeeq, "Viscosity, Refractive Index, Surface Tension, and Thermal Decomposition of Aqueous N-Methyldiethanolamine Solutions from (298.15 to 338.15) K," *J. Chem. Eng,* vol. 53, pp. 2226-2229, 2008.

Appendix A

 Risk evaluation performed for laboratory experiments is given in this appendix. Material safety data sheets of chemicals and NTNU HSE handbook are the basis of this assessment. Risk analysis was performed in collaboration of supervisor. Appropriate safety measure were suggested for identified potential hazards.

ID	5880		**Status**	**Date**
Risk Area	Risikovurdering: Helse, miljø og sikkerhet (HMS)		Created	18.02.2016
Created by	Asad Arif		Assessment started	18.02.2016
Responsible	Asad Arif		Actions decided	
			Closed	

EEART, Master student, 2016, Asad Arif

Valid from-to date:

2/14/2016 - 2/18/2018

Location:

Laboratories IKP (K4.216 - K4.220 - K4.218 - K4.U21-Chemistry Hall C)

Goal / purpose

Risk assessment of all the lab work during master thesis.

Background

- To perform gas permeation tests on membrane in gas rig (K4.218)
- Membrane preparation by solvent casting, deep and knife coating (K4.220 & K.216)
- To perform pervaporation test on membrane (Chemistry Hall C)
- To perform experiments on pressure decay rig

Description and limitations

Existing risk assessment for the equipment and activities:
- Gas permeation rigs
- Membrane preparation
- Pervaporation Setup
- Pressure Decay Rig

Prerequisites, assumptions and simplifications

Membrane preparation
The process involves small amount of chemicals, the MSDS illustrates process chemicals are non-toxic. The preparation carried out inside a fume hood using the lab safety equipment (lab coat, gloves, and goggles).
Refer to the membrane preparation procedure enclosed to the present assessment.

Pervaporation Setup
The process involves 0.5 to 1-liter aqueous amine solutions and water. The mandatory equipment is goggles, Lab coat, and mask (if amine is used). Gloves are used when handling amine solutions.

Pressure Decay Rig
The process involves 150ml liter pure amine, organic liquids, and water. The mandatory equipment is goggles, Lab coat, and mask (if amine or organic liquids used). Gloves are used when handling amine solutions.

The summary presents an overview of hazards and incidents, in addtition to risk result for each consequence area.

Hazard:	**Membrane Preparation**				

Incident:	**Inhalation of solvent**				

Consequence area:	Helse	Risk before actions:	🟢	Risiko after actions:	⚪

Hazard:	**Pervaporation**				

Incident:	**Spillage of chemicals**				

Consequence area:	Helse	Risk before actions:	🟢	Risiko after actions:	⚪
	Ytre miljø	Risk before actions:	🟢	Risiko after actions:	⚪

Incident:	**Liquid Nitrogen Spillage**				

Consequence area:	Helse	Risk before actions:	🟡	Risiko after actions:	⚪

Hazard:	**Vaccum Oven**				

Incident:	**Exhaust of solution vapor**				

Consequence area:	Helse	Risk before actions:	🟢	Risiko after actions:	⚪

Hazard:	**Pressure Decay rig**				

Incident:	**Inhalation**				

Consequence area:	Helse	Risk before actions:	🟡	Risiko after actions:	⚪
	Ytre miljø	Risk before actions:	🟢	Risiko after actions:	⚪

Overview of existing relevant measures which have been taken into account for this risk assessment

The table below presents existing measures which have been take into account when assessing the likelihood and consequence of relevant incidents.

Hazard	Incident	Mesaures taken into account
Membrane Preparation	Inhalation of solvent	Fumehood
	Inhalation of solvent	Personnel Safety Equipment
Pervaporation	Spillage of chemicals	Fumehood
	Spillage of chemicals	Personnel Safety Equipment
	Liquid Nitrogen Spillage	Personnel Safety Equipment
Vaccum Oven	Exhaust of solution vapor	Apparatus training
	Exhaust of solution vapor	User manual
	Exhaust of solution vapor	Fumehood
	Exhaust of solution vapor	Personnel Safety Equipment
Pressure Decay rig	Inhalation	Apparatus training
	Inhalation	User manual
	Inhalation	Fumehood

Existing relevant measures with descriptions:

Apparatus training
Proper training was received from equipment responsible

User manual
The user manual was studied before carrying out experiments.

Fumehood
The experiments were carried out in fume-hood to avoid any damage to human and environment.

commerical appartus
The risk analysis of SEM was already is carried out by the supplier.

Personnel Safety Equipment
Gloves
Goggles
Lab coat
Mask

Risk analysis with evaluation of likelyhood and consequence

This part of the report presents detailed documentation of hazards, incidents and causes which have been evaluated. A summary of hazards and associated incidents is listed at the beginning.

The following hazards and incidents has been evaluated in this risk assessment:

- **Membrane Preparation**
  - Inhalation of solvent
- **Pervaporation**
  - Spillage of chemicals
  - Liquid Nitrogen Spillage
- **Vaccum Oven**
  - Exhaust of solution vapor
- **Pressure Decay rig**
  - Inhalation

Overview of risk mitigating actions which have been decided, with description:

Membrane Preparation (hazard)

Membrane were prepared under fumehood

Membrane Preparation/Inhalation of solvent (incident)

Overall assessed likelihood of the incident: Unlikely (1)

Comment to likelihood assessment:

The was done under fumehood.

Assessment of risk for the consequence area: Helse

Assessed likelihood (common for incident):   Unlikely (1)

Assessed consequence: Small (1)

Comment to consequence assessment:

[Ingen registreringer]

Pervaporation (hazard)

Pervaporation /Spillage of chemicals (incident)

The spillage of Aqueous amine solutions. The MSDS illustrates possible harm to environment and humans.

Overall assessed likelihood of the incident: Less likely (2)

Comment to likelihood assessment:

[Ingen registreringer]

Assessment of risk for the consequence area: Helse

Assessed likelihood (common for incident):   Less likely (2)

Assessed consequence: Medium (2)

Comment to consequence assessment:

Amine are reported to be toxic if inhaled.

Pervaporation /Liquid Nitrogen Spillage (incident)

If Liquid nitrogen spilled on hand even in case of gloves can cause burn.

Overall assessed likelihood of the incident: Unlikely (1)

Comment to likelihood assessment:

[Ingen registreringer]

Assessment of risk for the consequence area: Helse

Assessed likelihood (common for incident):   Unlikely (1)

Assessed consequence: Large (3)

Comment to consequence assessment:

[Ingen registreringer]

71

Vaccum Oven (hazard)

Heating membrane at 200 C.

Vaccum Oven/Exhaust of solution vapor (incident)

The chemicals are non-toxic but process is carried out under fumehood.

Overall assessed likelihood of the incident: Unlikely (1)

Comment to likelihood assessment:

[Ingen registreringer]

Assessment of risk for the consequence area: Helse

Assessed likelihood (common for incident): Unlikely (1)

Assessed consequence: Small (1)

Comment to consequence assessment:

Chemicals are non toxic.

Pressure Decay rig (hazard)

inhalation of organic or amine vapours

Pressure Decay rig/Inhalation (incident)

Inhalation of the amine can be carcinogenic for humans in the long run mask is mandatory.

Overall assessed likelihood of the incident: Less likely (2)

Comment to likelihood assessment:

[Ingen registreringer]

Assessment of risk for the consequence area: Helse

Assessed likelihood (common for incident): Less likely (2)
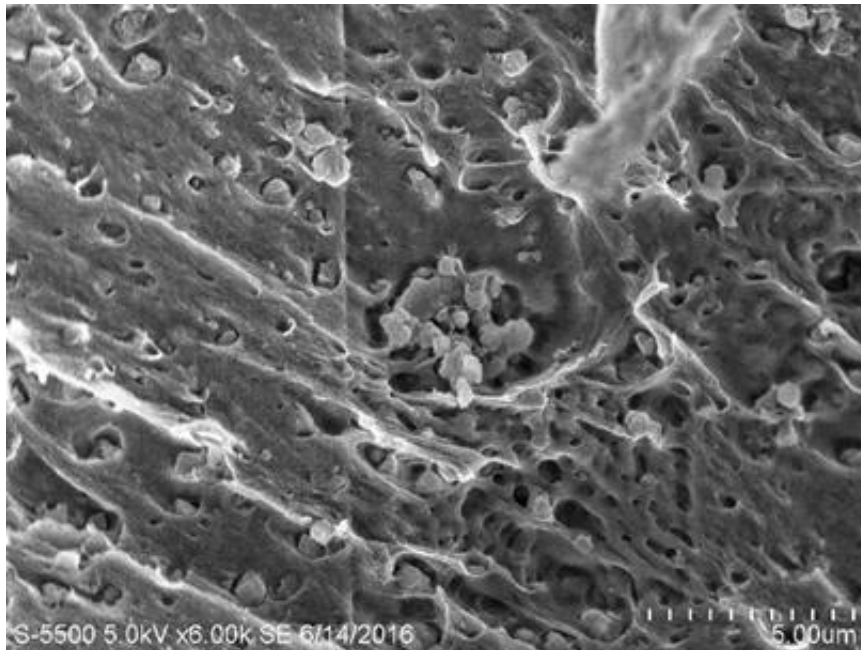
Assessed consequence: Large (3)

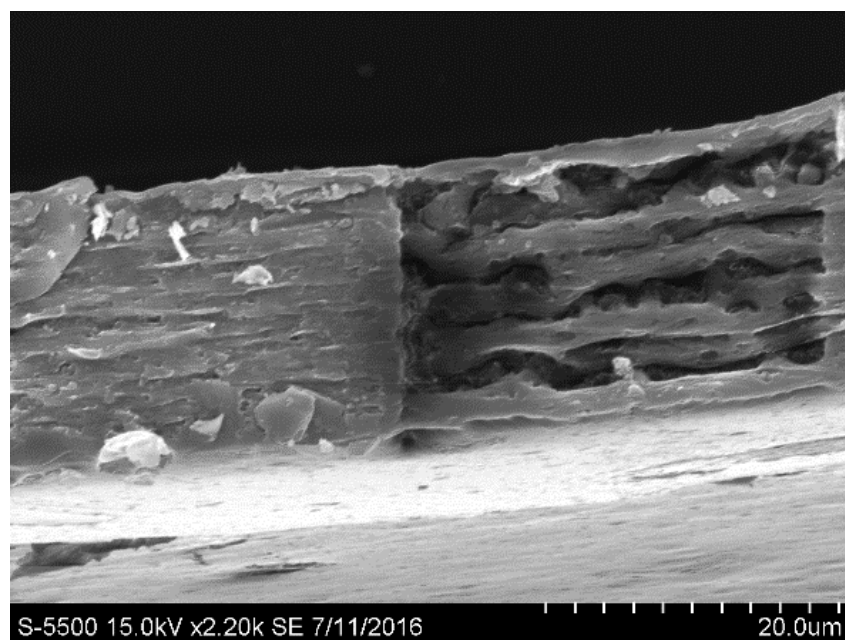Comment to consequence assessment:

[Ingen registreringer]

Appendix B

Another SEM image of Teflon AF2400 MMM with 10% loading of ZIF-8 are shown in **Figure 48**. The particle aggregation and voids are visible in diagram.

Figure 48: SEM Image of 10% ZIF- 8 Teflon AF2400

The SEM image in **Figure 49** shows the damage to the cross section at higher magnification and voltage.

**Figure 49:** SEM Images of 7.5% ZIF- 8 Teflon AF2400

Appendix C

Calibration of Gas permeation rig

The downstream volume has been preventively calibrated, and experiment done for apparatus of gas permeation rig. The overall model is called constant volume – variable pressure model.

	Offset	p1		p2		p3		known V	α	Downstream V
	offset mbar	mbar		mbar		mbar		cm3		cm3
1	27.8	815.2	787.4	202.6	174.8	160	132.2	76.0	2.414	183.5
2	26.9	777.7	750.8	194.1	167.2	154.3	127.4	76.0	2.488	189.1
3	27.4	739.9	712.5	186.2	158.8	148.4	121	76.0	2.488	189.1
4	27.6	713.8	686.2	180.3	152.7	143.2	115.6	76.0	2.423	184.1
5	27	922.4	895.4	227.9	200.9	178.9	151.9	76.0	2.404	182.7
6	28.3	567.1	538.8	148.3	120	118.9	90.6	76.0	2.395	182.0
7	27.6	853.2	825.6	212	184.4	167.6	140	76.0	2.449	186.1
8	28.3	834.7	806.4	208.1	179.8	164.4	136.1	76.0	2.420	183.9
9	28.3	460.8	432.5	124.9	96.6	101	72.7	76.0	2.362	179.5
10	28.1	746.1	718	188	159.9	149.6	121.5	76.0	2.459	186.9
11	27.8	411	383.2	113.1	85.3	92.8	65	76.0	2.489	189.2
12	27.3	400.2	372.9	110.3	83	90.5	63.2	76.0	2.481	188.6
13	27.5	677	649.5	172.2	144.7	136.9	109.4	76.0	2.409	183.1
14	27.5	617.8	590.3	160	132.5	128	100.5	76.0	2.436	185.1
15	27.4	598.3	570.9	155.3	127.9	124	96.6	76.0	2.395	182.0
16	28.1	284.5	256.4	85	56.9	70.9	42.8	76.0	2.362	179.5
17	28.1	395.9	367.8	109.5	81.4	89.4	61.3	76.0	2.375	180.5
18	27.3	540.2	512.9	141.7	114.4	114.2	86.9	76.0	2.455	186.6
19	28.3	505.5	477.2	134.6	106.3	107.9	79.6	76.0	2.317	176.1
20	27.5	406.3	378.8	112.6	85.1	92	64.5	76.0	2.428	184.5
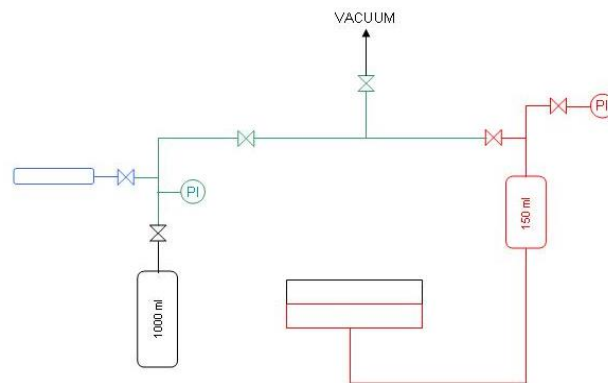
Figure 50: The depiction of single gas permeation rig

The image is depiction of whole process. The known volume V1 is attached to the gas permeation rig and a pressure sensor is attached on upstream side. The Valve for different sections opened and change in pressure in noted down and correspond volume is calculated.

Appendix D

The temperature dependence of permeability in polymeric dense membrane usually explained by Arrhenius equation explained:

$$P = P_o exp\left(\frac{-E_p}{RT}\right)$$

Taking natural log of Arrhenius Equation

$$\ln P = \ln P_o - \frac{E_p}{RT}$$

Plotting ln P versus 1/T (K) and the following results are shown in **Figure 51** and **Figure 52**. The slope was calculated from the excel with slope function, $\frac{E_P}{R}$ was obtained and to calculate the activation energy it was divided by the gas constant R. The obtained values of activation energies are shown in **Table 5**.
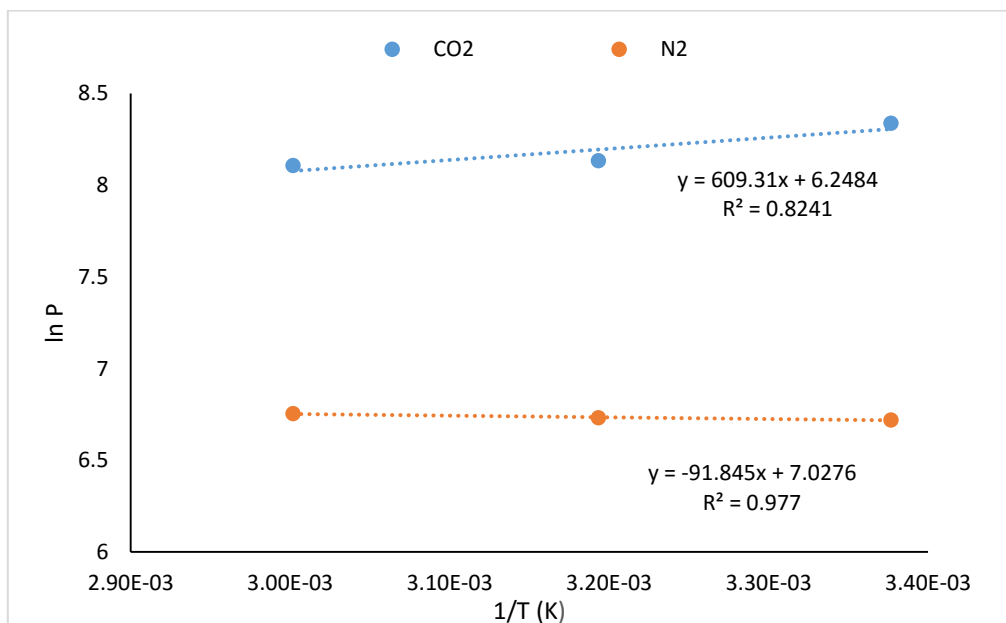
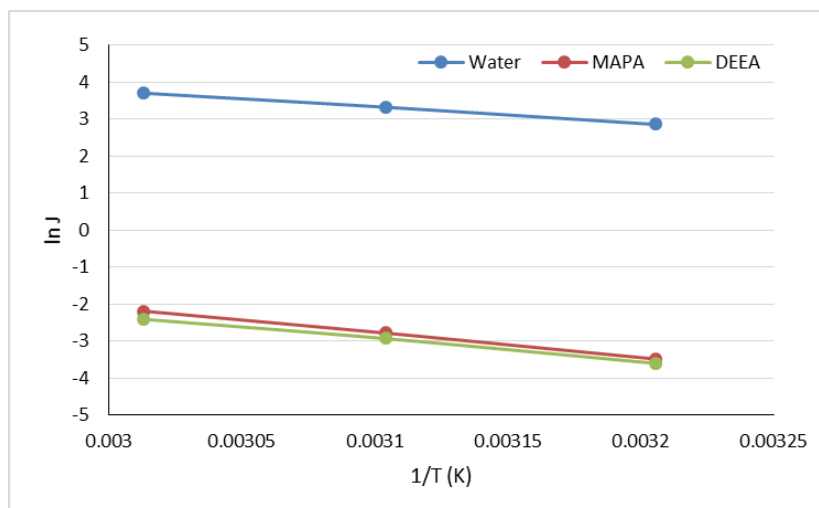**Figure 51:** Nat. log of permeability versus 1/T of 7.5% ZIF-8 & Teflon AF2400 MMM
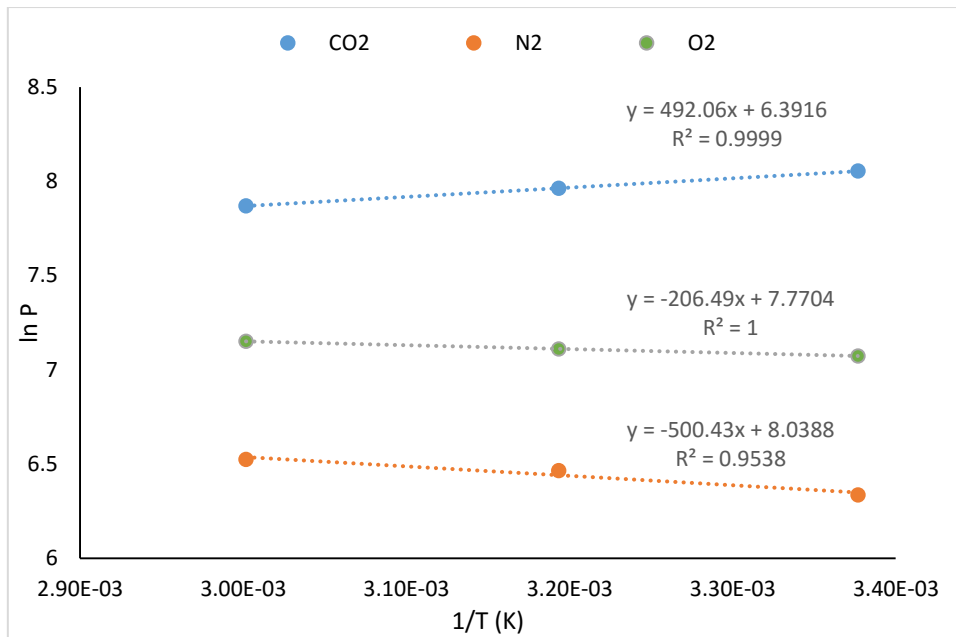
Figure 52: Natural log of permeability versus 1/T of pure Teflon AF2400

The kinetic size of 3rd generation amine is much larger than CO_2. The inclusion of nanoparticles will increase the diffusive path ways and it will lead to reduced flux for solvents. The Arrhenius plot for flux of 3D3M is shown in **Figure 53**.
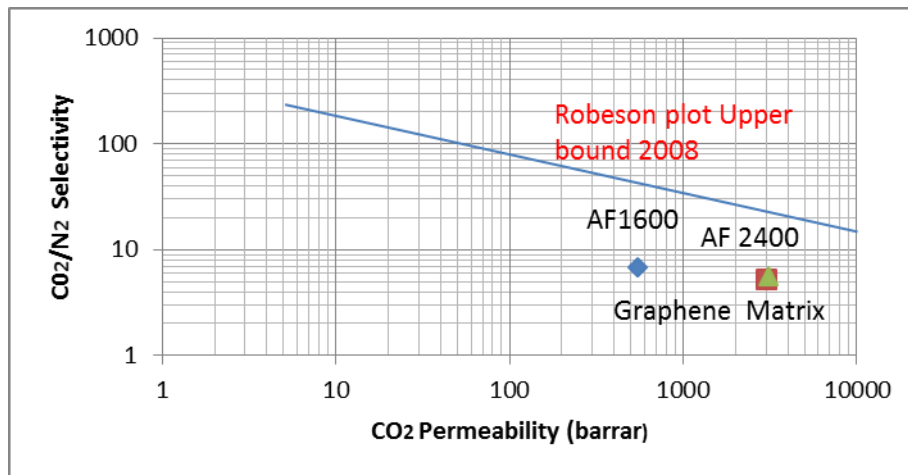

Figure 53 : Natural log of permeability versus 1/T of MMM

Appendix E

In the initial phase of the project, the graphene was studied as dispersion phase in Teflon AF2400 polymer matrix results are shown in **Figure 54**. The study concluded that graphene does not contribute to permeability but slightly selectivity decreased.

Figure 54: Robeson plot of CO_2 permeability versus CO_2/N_2 selectivity

Appendix F

Table 6: Fluxes of MAPA and DEEA for 3D3M solution at different operating temperatures in pure AF2400 and ZIF-8 7.5% MMM

Temperature (°C)	Flux (mol/hr/cm2*105)		Flux (mol/hr/cm2*105)	
	DEEA	DEEA	MAPA	MAPA
	AF2400	ZIF-8 7.5% MMM	AF2400	ZIF- 8 7.5% MMM
40	0.051	0.027	0.043	0.030
50	0.074	0.053	0.072	0.0617
60	0.195	0.090	0.188	0.111